1-1-2007

Experimental determination of solvent gas dispersion in vapex process

Randa E. El-Haj
Ryerson University

EXPERIMENTAL DETERMINATION OF SOLVENT GAS DISPERSION IN VAPEX PROCESS

by

Randa E. EL-Haj
Bachelor of Science
University of Khartoum
Khartoum, Sudan, 1995

A thesis
presented to Ryerson University
in partial fulfillment of the
requirement for the degree of
Master of Applied Science
in
Chemical Engineering

Toronto, Ontario, Canada, 2007

Instruction for Borrowers

Ryerson University requires the signatures of all persons using or photocopying this thesis.

Please sign below, and give address and date.

Name	Signature	Address	Date

Abstract

EXPERIMENTAL DETERMINATION OF SOLVENT GAS DISPERSION IN VAPEX PROCESS

Randa E. EL-Haj
Master of Applied Science, 2007
Department of Chemical Engineering,
Ryerson University

Canada has about one-third of the world's known petroleum reserves in the form of heavy oil and bitumen, which can meet our energy needs for the next two centuries. In this context, the vapor extraction (Vapex) of heavy oil and bitumen has drawn considerable attention in recent years. Not only this process has the potential to sequester greenhouse gases besides requiring low energy costs and capital investment, but also the capability of in situ upgrading of heavy oil. At present, there is a significant interest in the determination of the dispersion of solvent gases during Vapex in order to predict the amount and time scale of oil recovery as well to optimize the field operations. Not much research has been done so far to investigate dispersion in presence of fluid flow that is transverse to gravity such as in Vapex. In this work, the dispersion of butane solvent gas is determined as a linear function of its concentration in heavy oil and bitumen based on Vapex experiments carried out in the Transport Modeling Laboratory at Ryerson University. A cylindrical wire mesh, which had a cavity of 21 cm high and 6 cm diameter, packed with homogeneous porous media saturated with Athabasca heavy oil was used as a physical model for heavy oil vapor interface. The physical model was

packed with three different sizes of glass beads. The permeabilities of the different homogeneous glass beads packing were tested. For each model, an experiment was conducted at a room temperature with $\pm 0.5\,^{\circ}C$ variation, and pressure close to butane dew point with variation $\pm$ 0.007 MPa. Under these conditions, the physical model was exposed to a butane solvent gas, which diffuses into physical model, and gets absorbed in Athabasca bitumen. As a result of the gas absorption, a significant reduction in viscosity was experienced. The diluted live oil was drained along the solvent vapor/oil interface under the action of gravity. The decrease in mass of the physical model was measured and recorded every 1 minute. Average live oil viscosity, average density, and average dissolved butane mass fraction in Athabasca bitumen sample were determined to be 2.742 cP, 0.86 g/cm^3, and 0.48 respectively.

These experiments were simulated by a mathematical model, which was used to determine the dispersion coefficient of butane gas into Athabasca bitumen. The dispersion coefficient of the butane gas was considered as a linear function of its concentration in the porous media. The mathematical model was numerically solved using finite difference method. Different values for dispersion coefficient and butane saturation mass fraction were used in the simulation. Steepest decent method was used to iteratively evaluate dispersion coefficient and minimize the error. The optimum values of dispersion coefficient and butane gas saturation solubility in Athabasca bitumen were determined by matching the calculated and experimental values of live oil production.

Acknowledgment

I would like to extend my sincere thanks to everyone provided me help, support and courage throughout this study in every possible way.

My special thanks go to Prof. Ali Lohi for giving me an opportunity to work on this research and for his support with meaningful discussions, invaluable advices and rich ideas.

I am extremely indebted to Dr. Simant R. Upreti for his excellent supervision and inspiration throughout the thesis work. From his instruction, I learned the arts and skills of a researcher and more importantly the way of thought.

I appreciate the indisputable support that I received from the mechanical workshop team Mr. Peter Scharping and Mr. Ali Hemmati during the lab setup. I also appreciate the support I received from the electrical lab supervisor - Mr. Tondar Tajrobehkar.

I extend my thanks to my friends Chandra Adimoolam and Li Wan in appreciation of their helping hands at the hours of necessity. I would like to acknowledge also the useful suggestions of my colleagues Baitao Jiang, Amar Weli, and Rakesh Patel.

Finally and most importantly, this thesis is dedicated to my parents, my dearest daughter, and my lovely husband whose continuous backing and encouragement made this possible.

Table of Contents

List of Tables

List of Figures

Nomenclature

D	Diffusivity, m^2/s
D	Dispersion coefficient of butane gas in heavy oil and bitumen, m^2/s
D_0	D when $\omega = 1$, m^2/s
v	Darcy velocity, m/s
e_{rms}	Root mean square error
j_g	Mass flux of the gas, kg/ m^2s
K	Permeability of the physical model, m^2
K_r	Relative permeability of the physical model, m^2
m_{cal}	Calculated mass of produced live oil, kg
m_{exp}	Experimental mass of produced live oil, kg
g	Gravitational acceleration, m/ s^2
t	Time, h
Z	Height of the cylindrical model, m
Z_0	Height of the cylindrical model at (t = 0), m
R	Radius of cylindrical physical model, m
V	Volume of the differential element $(2\pi r\Delta r\Delta z)$, m^3
S	Differential area along r-direction $(2\pi r\Delta z)$, m^2
A	Differential area along z-direction $(2\pi r\Delta r)$, m^2
Q	Live oil production rate, $m^3/h.m$
d_0, d_1	Constants in equation (2.9)
T	Temperature, °C

N	Number of experimental data points
N_i	Number of grid points along r-direction
N_j	Number of grid points along z-direction
C	Solvent/heavy oil concentration
K_l	Longitudinal and transverse dispersion coefficient
K_t	Transverse dispersion coefficient
h	Reservoir height, m
S_0	Oil saturation

Greek Symbols

ω	Mass fraction of gas in bitumen
ω_{sat}	Saturated mass fraction of gas in bitumen
ϕ	Porosity of the physical model
μ	Viscosity of heavy oil and bitumen, kg/m.s
μ_0	Viscosity coefficient of heavy oil and bitumen, kg/m.s
Δr	Distance between grids along r-direction
Δz_i	Distance between grids along z-direction for a given r location
θ	Angle between the physical model and the horizontal, rad
α	Coefficient for the viscosity dependent diffusivity (Hayduk and Cheng, 1971)
β	Exponential coefficient for the viscosity dependent diffusivity (Hayduk and Cheng, 1971)
ρ	Density of the live oil, kg/m^3

1 Introduction

Petroleum is the world's primary energy source and is a key factor in the continued development of world economies. Petroleum reserves are classified as conventional and unconventional based on their viscosities and API gravities. The viscosity of conventional reserves is lower than 100 cP with API gravity of 20° or greater, while unconventional reserves have viscosity greater than 100 cP with API gravity of 20° or less (Figure 1.1). Conventional reserves are typically the highest quality, lightest oil, which flow from underground reservoirs with comparative ease. Unconventional reserves are heavy and often tar like, and include oil shale, tar sands/bitumen, heavy and extra-heavy crude oils, and deep-sea oils.

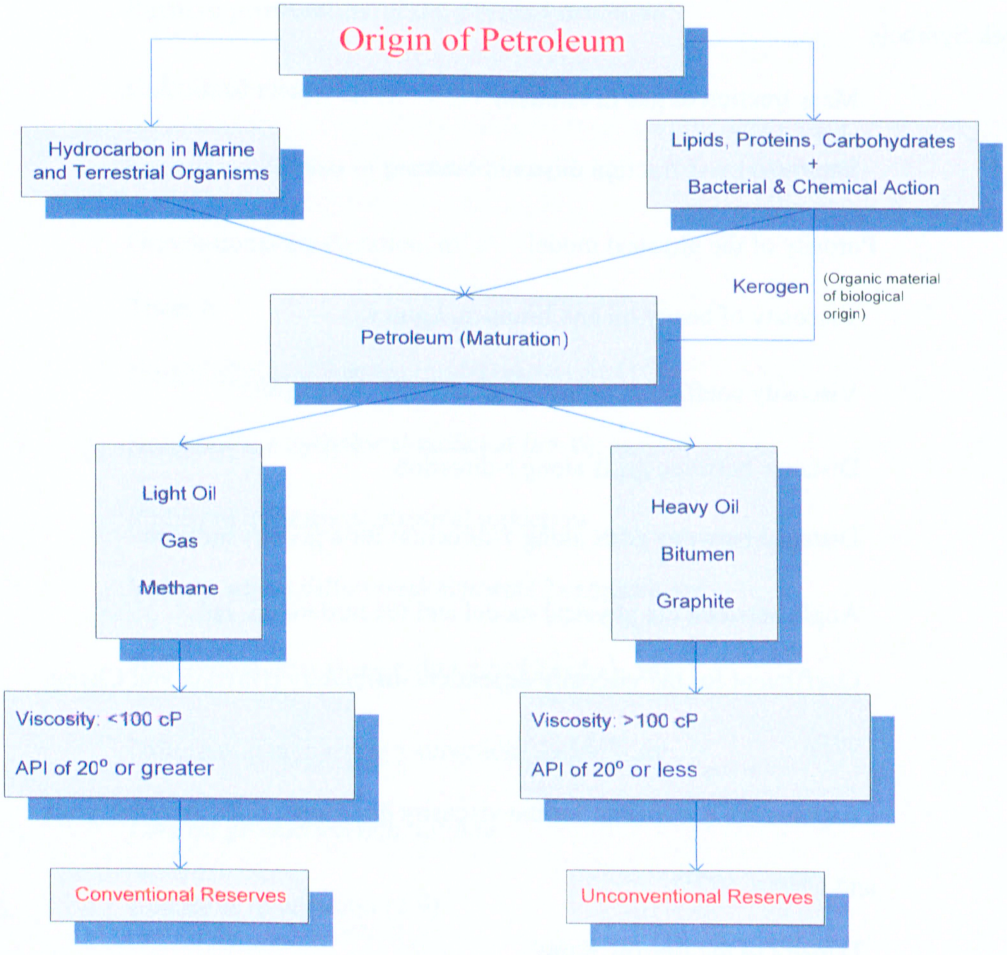

Figure 1.1 Origin of Petroleum

As shown in Figure (1.2), the worldwide global demand for oil has grown by 150% since 1965 and is projected to grow by another 50% in the next 20 years (Isaacs, 2005). The growth in global demand for oil comes at a time when the supply from relatively cheap conventional sources is declining, and new reservoir discoveries have become rare. To sustain the increasing worldwide demand of petroleum products, the gap between oil demand and supply must be met by developing alternative sources of oil from indigenous resources. An attractive alternative in this context is the recovery of heavy oil and bitumen.

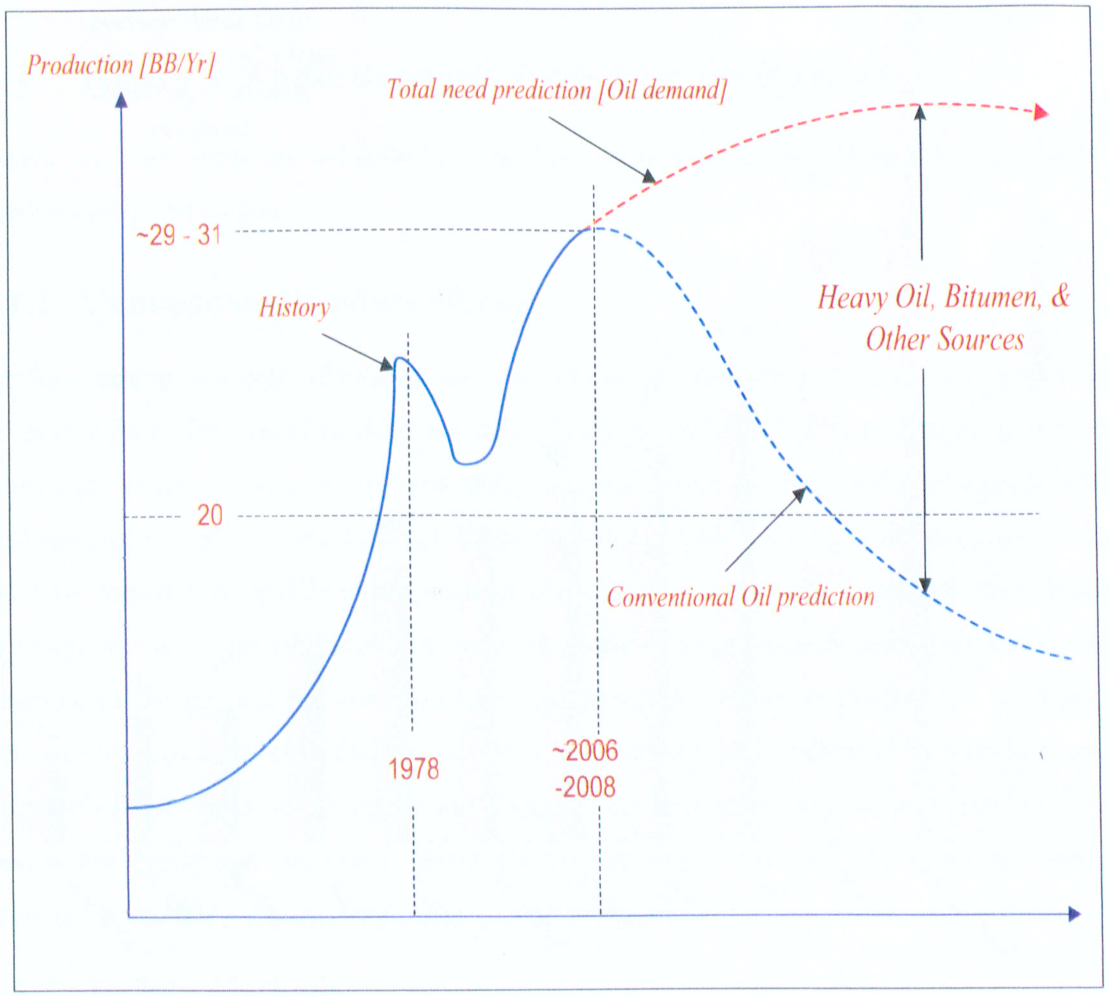

Figure 1.2 Conventional Oil Production and Oil Demand

(Dusseault B. M., 2002)

Canada has over 175 billion barrels of recoverable heavy oil and bitumen reserves (Figure 1.3). These vast reserves make Canada second only to Saudi Arabia as an oil resource country. However, the main difficulty in the oil recovery from these vast reserves is their immobility under reservoir conditions due to their high viscosity (10^4–10^6 cP or even higher) (Das and Butler, 1996).

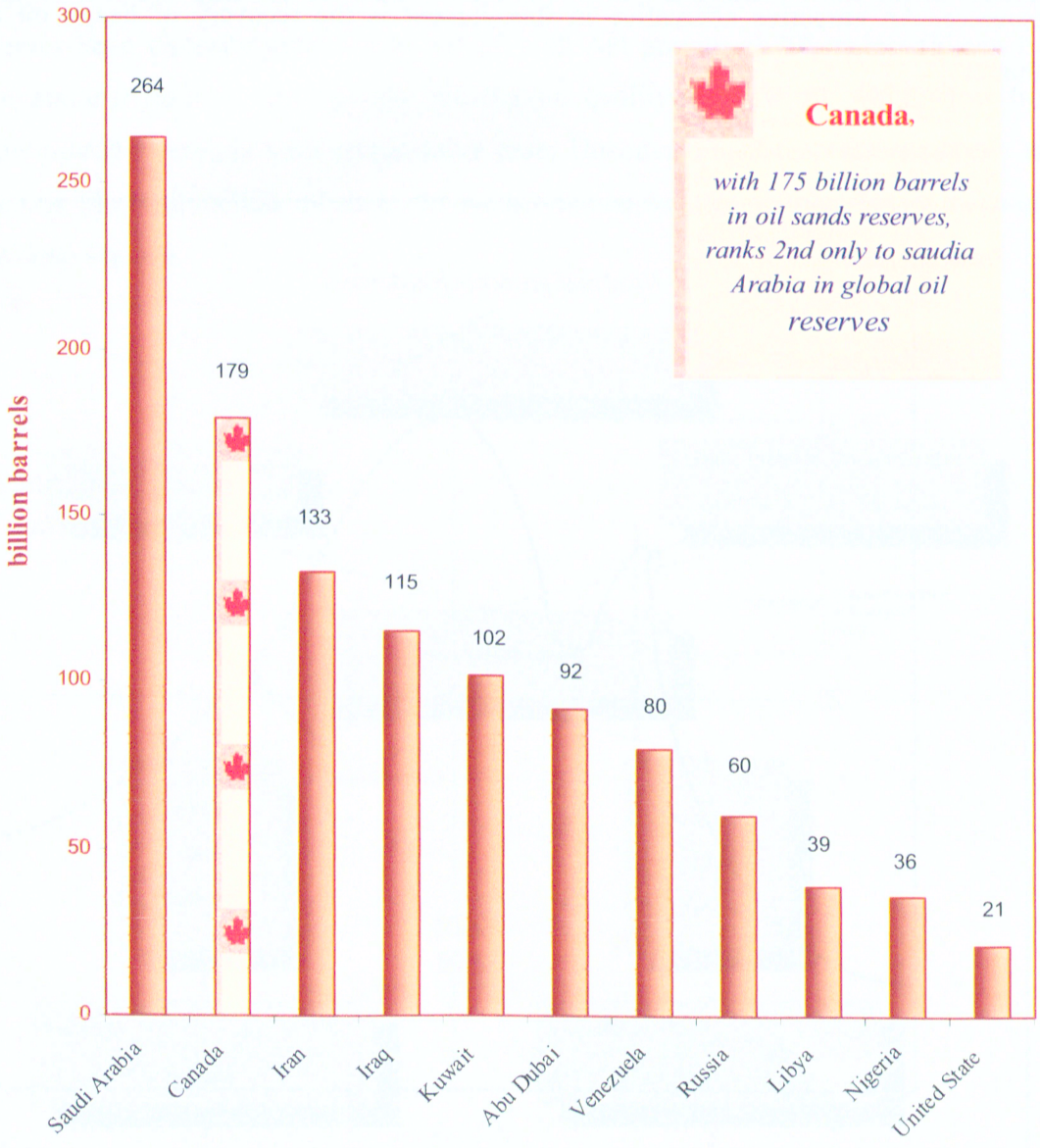

Figure 1.3 Global Crude Oil Reserve by Country

(Oil & gas Journal, 2005)

Heavy oil and bitumen reserves often results from a bacterial oxidation of conventional oils inside the reservoir rocks, thereby resulting in varied physical and chemical oil properties. Unconventional reserves have high asphaltene, high heavy metals, and sulfur and nitrogen contents. Due to the extremely high viscosity of heavy oils and bitumen at reservoir conditions, their mobility or ability to flow through the porous media is very low. Thus, the primary production of these oils is very difficult and the recovery ratio is generally low, less than 10%. Therefore, production of unconventional reserves implies specific technological solutions for production, in order to make the exploration of this unconventional crude more economical, and to reduce substantially the associated environmental impacts.

1.1 Heavy Oil and Bitumen Recovery Techniques

Heavy oil and bitumen exploration currently incorporates two production methods: conventional and in-situ.

1.1.1 Conventional Surface Mining

Surface mining is a type of mining used to extract bitumen accumulations that are close to the surface. This process involves digging up the oil sand then transporting it to a treatment facility where it will be subjected to steam or hot water treatment and centrifuging to separate the bitumen from the sand (Figure 1.4). Four tones of oil sands must be mined and processed to produce one cubic meter of oil. Although 75% of the bitumen in place can be recovered from the sand; the processed sand then has to be returned to the pit and the site reclaimed. To date, the maximum overburden thickness that can be removed economically is about 75 m otherwise it requires the handling and disposal of vast amounts of solids and sludge. The surface mining method also leaves a devastated landscape requiring reclamation. The major part of Canadian oil sands resource is too deeply buried for mining to be practical.

1.1.2 In-Situ Methods

In-situ methods involve improving the flow of oil by changing the properties of the heavy oil and bitumen, the predominant mechanism of these methods is viscosity reduction.

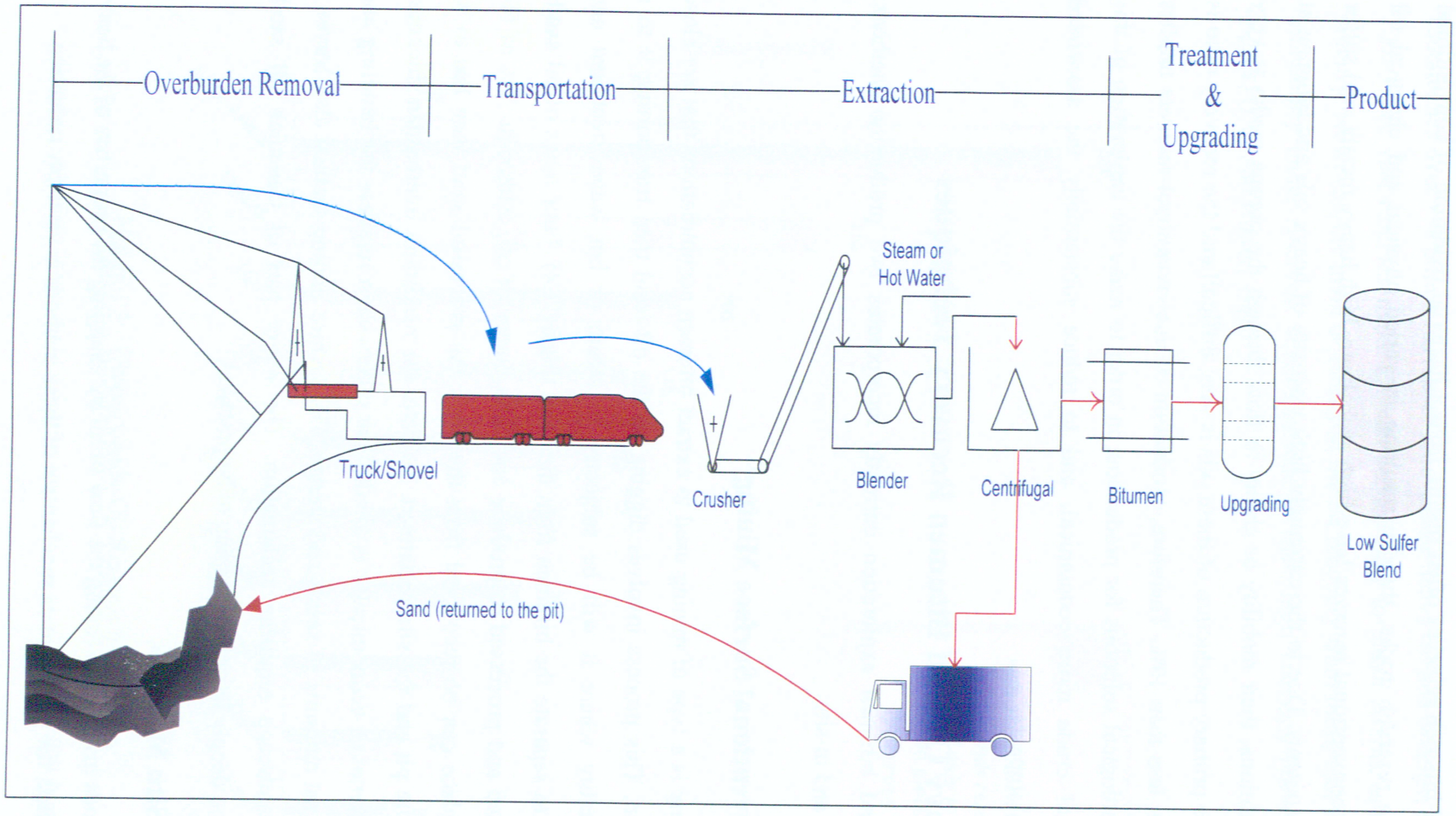

Figure 1.4 Schematic Diagram of Conventional Methods

These methods are used for heavy oil and bitumen that are too deep to support cost-effective surface mining operations. There are two types of in-situ enhanced oil recovery method: thermal and non-thermal. Thermal methods are the most widely used and well known for dramatic heavy oil viscosity reduction. In these methods, the viscosity is reduced by increasing the reservoir temperature by the heating the reservoir rock (Figure 1.5).

1.1.2.1 Thermal Recovery Methods

In thermal processes, hot water or steam is injected into wells where it contacts the oil. As the steam condenses, latent heat is transferred to the reservoir, decreasing bitumen viscosity until it is able to flow to the production well. Cyclic Steam Stimulation (CSS) and Steam Assisted Gravity Drainage (SAGD) are the most common thermal recovery methods.

In the CSS or "huff-and-puff" method, the well is put through cycles of steam injection, soak, and oil production. First, steam is injected into a well, at a temperature of 300 degrees Celsius, for a period of several weeks or months. The well is allowed to sit for several days to let heat enter the oil sands. The hot bitumen is then pumped out of the well, which may take weeks. When the production rate falls, the well is put through several more cycles of injection, soak, and production, until the cost of injecting steam exceeds production costs. Maximum recovery seldom exceeds 20% OOIP (Das, 1997). For cyclic steam stimulation three to eight barrels of steam are required to produce one barrel of oil, this relationship known as steam/oil ratio (SOR).

In a typical SAGD (Steam Assisted Gravity Drainage) approach steam is injected into the reservoir at high temperature and pressure through a horizontal well located directly above a horizontal producer. Heat is transferred by latent heat of the steam. By injecting steam, a steam chamber forms directly above the production well. At the steam chamber boundary, steam condenses to water as heat is transferred to the oil. The hot oil, that is less viscous, drains by gravity to the production well. SAGD is cheaper than CSS, allows very high oil production rates, and recovers up to 60% of the oil. Typical steam/oil (SOR)

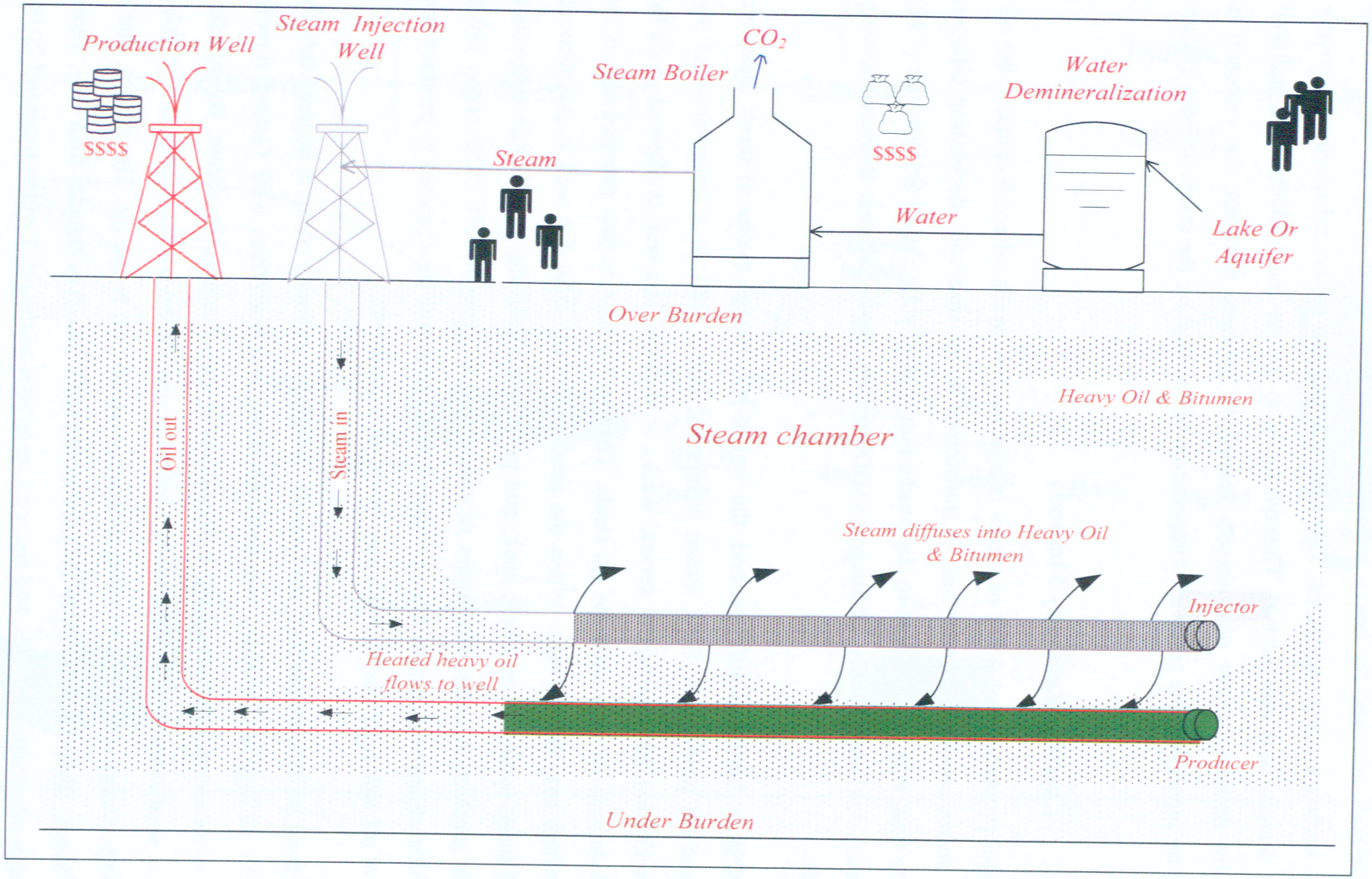

Figure 1.5 SAGD View – Vertical Cross Section along Well (Thermal Recovery Methods)

values for steam assisted gravity drainage are in the range of three to five.

Despite the higher recovery expected from thermal methods especially SAGD process, the huge amount of energy required, higher greenhouse gas emissions and much higher production costs results in major drawbacks. In addition to that any steam injection process becomes more difficult to operate in a thin reservoir where heat losses to the base and the cap rock makes the injected steam/oil produced ratio prohibitively high. Therefore, thermal processes becoming economically non-feasible in reservoirs that have the following properties: low thermal conductivity, bottom water, high water saturation, vertical fractures and/or fissures, low porosity. Consequently, there is a huge amount of unconventional resources present in such reservoirs that can be exploited with new technologies.

1.1.2.2 Non Thermal Recovery Methods

Demanding far less energy than SAGD, the non thermal methods is the next alternative. The Cold Heavy Oil Production with Sand (CHOPS) and the Vapor Extraction Process (Vapex), as non-thermal recovery methods for heavy oil and bitumen have recently gained considerable attention and promise as an alternative to thermal methods for the recovery of heavy oil and bitumen reservoirs that are deemed unsuitable for thermal methods.

Cold Heavy Oil Production with Sand (CHOPS) process is a pressure driven process, in which both heavy oil and sand are pumped out to the surface using a specialized pump called progressive cavity pump. This process has been economically successful in several heavy oil fields in Alberta and Saskatchewan (Dusseault B. M., 2002). The extraction of sand creates a wormhole network and a foamy oil drive. These two effects are the main influences in enhanced oil recovery. This extraction causes high pressure gradients in the reservoir resulting in the failure of the unconsolidated sand matrix. The simultaneous extraction of oil and sand during the cold production of heavy Oil generates high permeability channels termed "wormholes". The development of wormholes causes reservoir pressure decrease to the bubble point and as the pressure falls below the bubble

point, the dissolved gases appear as bubbles within the oil. The viscosity and specific gravity of heavy oil restrict the gas bubbles from separating into a single phase resulting in what is known as foamy oil. This process increases the fluid volume within the reservoir, forcing grains apart, and providing pressure to sustain the high production rates. This method only works well in areas where the bitumen is fluid enough to pump. The advantage of this method is good production rates and recovery (around 10%) and the disadvantage that disposing of the produced sand is a problem.

Vapor Extraction (Vapex) of Heavy Oil and Bitumen is a promising recovery technology that involves the injection of solvents into the reservoir, vapor dissolves in the high viscosity oil at the interface and diffuses through it; the viscous oil gets diluted and drains to the horizontal production well by gravity (Figure 1.6). Vapex is a non thermal method where the bitumen is fluidized by molecular diffusion of the light hydrocarbon which acts as a solvent instead of thermal diffusion as in steam processes.

Performance of Vapex process is directly related to the amount of solvent dissolving into the bitumen. Therefore, similar to SAGD, two horizontal wells are used in the Vapex process to expose a larger area of the reservoir to the wellbore thereby increasing the productivity and to reduce the drawdown. The higher area of contact between solvent vapor and the crude yield higher rate of mass transfer of the solvent and higher recovery (Das and Butler, 1996).

The predominant mechanism for Vapex process is the diffusion of solvent into the heavy oil and bitumen. Production rates are directly related to viscosity reduction, which in turn depends on the amount of solvent dissolved in the crude. Mixing of the solvent with heavy oil and bitumen is slow because it occurs only when solvent diffuses through the pores. Compared to SAGD, the heating of reservoirs is much faster because heat can be carried through at relatively high thermal conductivity rock as well as in the pores (Butler and Yee, 2002); this thermal diffusion is much faster than the molecular diffusion required for solvent mixing. Therefore, it is generally expected that Vapex production rates will be much lower than those in a steam process.

Solvent selection is a critical economic factor in Vapex. The ideal solvent depends on

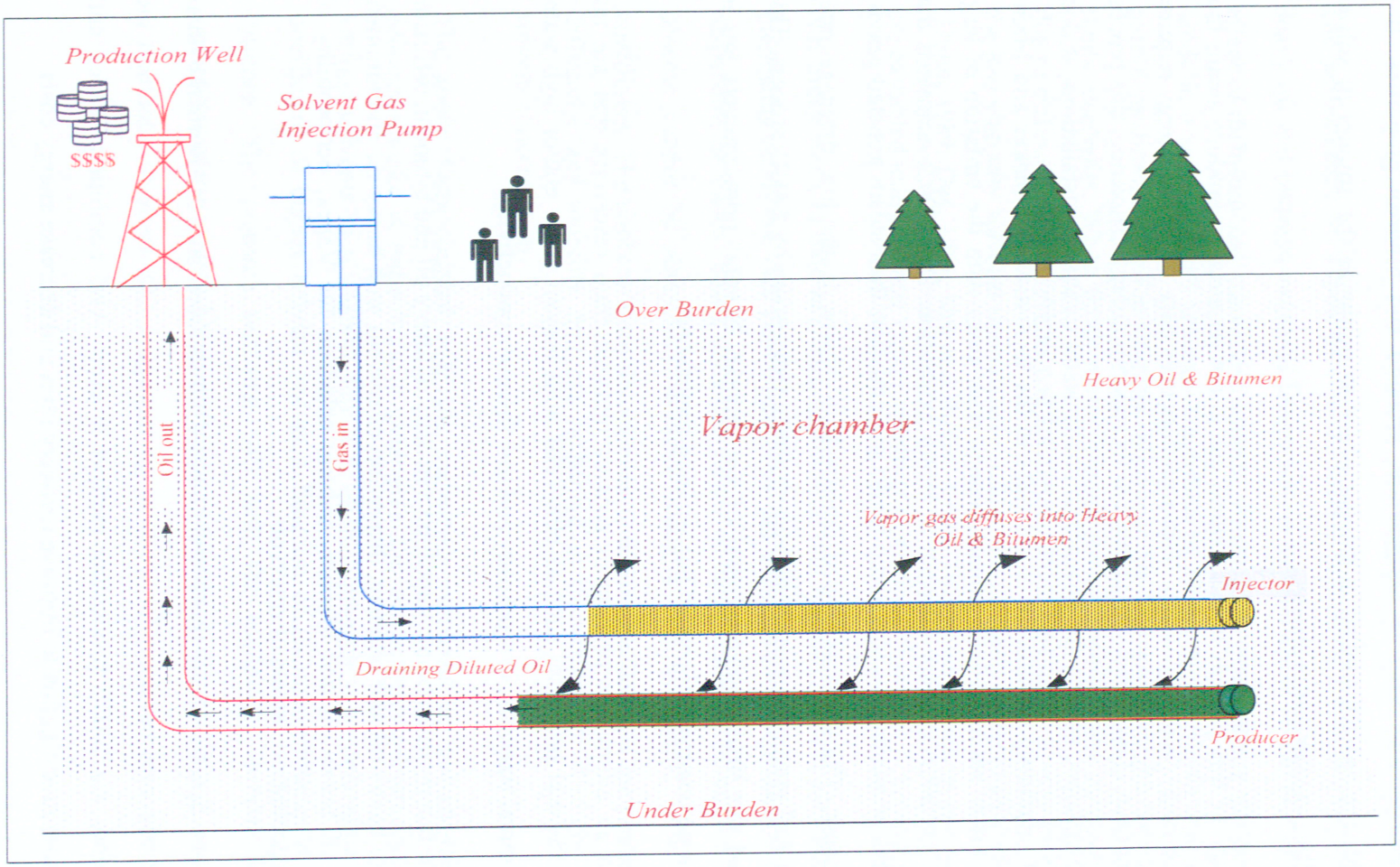

Figure 1.6 Vapex View – Vertical Cross Section along Well (Non Thermal Recovery Methods)

reservoir characteristics such as temperature, pressure and bitumen properties. It is important that the solvent remain in the gas phase to minimize the amount of solvent required to fill evacuated pore spaces.

The advantage of this process is that natural gas is not required to produce steam thus providing a savings on energy usage. Vapex process uses only 3% of the energy required by steam processes (Das, 1998). In addition to its superior energy efficiency, this process has many advantages, notably the absence of costly water treatment installations; it does some partial upgrading of bitumen to oil right in the formation (Karmaker and Maini, 2003) and a lower environmental impact. Vapex does away with the emission of large quantities of greenhouse gases inherent in steam generation. Das (2002) estimated that Vapex process produces 80% less green house gas emission than steam assisted gravity drainage process. The main perceived drawback of Vapex is the low drainage rates predicted for real reservoirs.compared with drainage rates given by SAGD process. This has hampered the field implementation of the process. Several pilot projects are in operation, but no commercial project has yet been announced.

Vapex offers an alternative process to recover bitumen from reservoirs that are not amenable to thermal processes such as reservoirs with bottom water and/or high water saturation, vertical fractures, low porosity and low thermal conductivity.

The important factors influencing Vapex are viscosity of heavy oil and bitumen, diffusion of solvent into heavy oil and bitumen, dispersion of solvent with heavy oil and bitumen, deasphalting of heavy oil and bitumen, solvent selection for Vapex, permeability of reservoir and geological factors of reservoir.

In order to get benefit of all these technologies advantages and to overcome their drawbacks, it becomes common for wells to go through a CSS cycle to condition the formation before the SAGD production method is used. Also combining Vapex and SAGD was under investigation to improve recovery rates and decrease energy costs.

1.2 Objective and Motivation of this Study

The performance of Vapex process is directly related to the dispersion of solvent into heavy oil and bitumen reserves. Dispersion is the mixing of fluids due to the combined effect of diffusion and convective motion, which takes place during the extraction of oil sands in a solvent-based process. Described by Darcy law at a macroscopic scale in a porous medium, dispersion strongly influences the recovery from the typically porous oil sands reservoirs. When fluids move through porous media, mass transport exceeds that due to diffusion alone (Perkins and Johnston, 1963). This effect is very pronounced when the low viscosity solvents dramatically reduce the viscosity of the highly viscous reserves (Dunn, 1989; Das, 1995; Das and Butler, 1998). This phenomenon occurs when oil sands are extracted using solvent vapors resulting in the fluid flow that is transverse to gravity.

Not much work to date has been reported in this regard (Yazdani and Maini, 2005). An interesting study by Das (2005) indicates the concentration-dependence of solvent gas dispersion in Vapex. Using different values of dispersion coefficient, he found that the process cannot be adequately modeled using a bulk (constant) value of dispersion coefficient. The concentration-dependence is reasonable because the phenomena such as diffusivity and mobility that are embodied in dispersion are strongly influenced by solvent concentration.

The above facts coupled with the increasing emphasis on solvent-based extraction processes make it imperative to determine the concentration-dependent dispersion of various solvents in oil sands. The aim of this research is to determine the dispersion coefficient of butane solvent gas as a function of its concentration in heavy oil and bitumen. The research outcome will help the modeling, simulation and optimal operations of the solvent-based extraction processes.

2 Literature Review

For years, the composition variation of the hydrocarbon components in reservoirs has been mystery. There are four distinct mechanisms, which influence the variation of composition in a single-phase two component system. These mechanisms are molecular diffusion, natural convection, thermal diffusion and pressure diffusion. For high permeability natural convection is the main phenomenon that affects compositional variation within the reservoir and results in a nearly homogeneous system (Ghorayeb and Firoozabadi, 2001).

In the reservoirs, the estimation of the rate of mass transfer caused by molecular diffusion and convective dispersion is necessary to determine (i) the amount and flow rate of gas required for its injection to a reservoir, (ii) the extent of heavy oil and bitumen reserves that would undergo viscosity reduction, (iii) the time required by the reserves to become less viscous and more mobile as desired, and (iv) the rate of live oil production from the reservoir. Hence, the diffusivity of gases in heavy oil and bitumen is an important consideration in enhanced oil recovery processes. For example, the performance of Vapex is directly related to the amount of solvent dissolved into bitumen. Solvent vapor diffuses into oil through the interface of the vapor chamber to form a mixed layer in which solvent concentration within the medium varies gradually. The solvent concentration within the crude oil depends on the vapor liquid equilibrium at the solvent-oil interface, and on the diffusion of solvents within the liquid. The concentration of solvent in the oil controls viscosity reduction, which consequently governs the dynamics of the live oil flow and production rates. One limitation of a solvent extraction process is the slow live oil production rates, which is mainly controlled by the molecular diffusion. This phenomenon continues to challenge the field implementation of such processes.

The experimental molecular diffusivities of solvent gases in heavy oil and bitumen are of the order 10^{-9} - 10^{-11} m^2/sec (Schmidt, 1989; Uprtei, 2000). On the other hand, the molecular diffusivities of solvent liquids could be higher in order of 10^{-7} m^2/sec (Schmidt, 1989). The fluid convection in permeable rocks can increase mass transfer rates by 2-3

orders of magnitude. When fluids move through porous media, mass transport exceeds that due to diffusion alone (Perkins and Johnston, 1963). The pressure gradient in the fluid, fluid viscosity and the specific permeability of the rock are dominant in determining the fluid velocity and mass transfer rates. Thus, fluid flow in porous media is a very complex phenomenon, and as such cannot be described as explicitly as flow through pipes or conduits. It is rather easy to measure the length and diameter of a pipe and compute its flow capacity as a function of pressure. In porous media, however, the flow is different in that there are no clear-cut flow paths to be measured. Considerable efforts have been made by several authors in the past years to understand the mass transfer of different gases in heavy oil and bitumen. This chapter highlights those efforts.

2.1 Diffusion of Solvent Gases in Heavy Oil and Bitumen

Diffusion is a molecular phenomenon reserved for the spreading of solvent molecules among the solute molecules. Concentration gradient and random motion must coexist for diffusion to occur. There are several theories for estimation of diffusion coefficients for liquids and gases in the literature. Many of these theories are built around the kinetic phenomena in liquids. However, none of these theories is quite satisfactory in predicting the diffusivities for bitumen system because of the arbitrary assumptions involved in treatment of kinetic phenomena in liquids (Oballa and Butler, 1989)

Several authors have developed diffusion correlations based on molecular theory. They used the Stokes Einstein equation, which relates the diffusion coefficient to viscosity as being inversely proportional to each other.

Hayduk and Cheng (1971) assumed that the diffusivity of a particular dilute species in any solvent depends only on the solvent viscosity, provided that the state of molecular aggregation of both the solute and solvent remains unaltered on mixing. They gave a relationship between diffusivity and viscosity involving two constants α and β which are characteristic for each diffusive substance:

$$D = \alpha \mu^{-\beta} \qquad (2.1)$$

Hayduk and Cheng (1971) tested this relation by using diffusivity data for eleven different solutes in a variety of solvents at various temperatures. They concluded that this relation is independent of temperature and solvent composition. The dependence of diffusivity on temperature and composition appears through the viscosity, which is known to be a strong function of temperature and solvent composition.

Hiss and Cussler (1973) studied the diffusion of small molecules in dilute solutions (solute mass fraction ≈ 0.003) in liquids having a wide range of viscosities. They measured diffusivities of hydrocarbon oil mixtures with viscosities in the range of 0.5 to 5,000 cp. They observed that at viscosities above 5 cP, $D\mu^{2/3}$ is constant and the following relation for diffusivity and viscosity was suggested

$$D = \alpha\mu^{-2/3} \tag{2.2}$$

Hayduk et al. (1973) measured diffusivities of propane in dilute solutions at different temperatures using the steady state capillary cell method. The effective diffusivity of propane was considered to remain constant along the diffusion path. Hence, the diffusivities calculated represent the integral average diffusivities corresponding to the average concentration along the diffusion path. The relation between log D and log μ was found to be linear and the equation describes this relationship was:

$$D = 0.591 \times 10^{-10}\mu^{-0.545} \tag{2.3}$$

Hayduk and Minhas (1982) presented a correlation for estimating the molecular diffusion coefficient of paraffin solute/solvent pair as follows

$$D = 13.3 \times 10^{-8} T^{1.47} V_a^{0.71} \mu^{\left(\frac{10.2}{V_a} - 0.791\right)} \tag{2.4}$$

This correlation expresses diffusivity as a function of temperature T, molar volume of the solvent (propane) V_a and the viscosity of the medium where diffusion occurs.

Das and Butler (1996) developed an empirical correlation for diffusivity of propane and butane on the basis of Vapex experiment in Hele-Shaw cell for the Peace River bitumen as a function of mixture viscosity, which in turn is a function of gas concentration and

temperature. Based on Hayduk and Cheng (1973) correlation, they obtained the optimized constant values for α and β for propane and butane to measure the diffusion coefficients as follows:

The empirical correlation for butane was:

$$D_s = 4.13 \times 10^{-10} \mu^{-0.46} \quad (2.5)$$

However, a different value of α was obtained for propane and the correlation was:

$$D_s = 1.306 \times 10^{-9} \mu^{-0.46} \quad (2.6)$$

Where D_s is the diffusion coefficient (m^2/s) and μ is the viscosity of the live oil in (Pa.s)

Table (2.1) indicates some of the available correlations for diffusivity estimation

Diffusivity of gases as a function of its concentration is normally correlated on the basis of the Fick's first law which defines diffusivity as a proportionality constant relating the mass flux of a species to its spatial concentration gradient opposite to the flux at a given temperature and pressure as follows:

$$j = -D\nabla C_A \quad (2.7)$$

where j is the mass flux of the species at its concentration C, and D is the diffusivity of species. The diffusivity defined by equation (2.7) is called Fick diffusivity.

Upreti and Mehrotra (2000, 2002) used indirect non-intrusive pressure decay experimental method to find the Fick diffusivity of CO_2, CH_4, C_2H_6, and N_2 gases in Athabasca bitumen. They observed that diffusivity is a function of gas concentration in bitumen, and at a given gas concentration and pressure, diffusivity increases with temperature. Their results indicate that gas diffusivity generally increases with pressure at a given temperature and gas concentration. They estimated the diffusivity of these gases in Athabasca bitumen, in the temperature range of 25–90°C at pressure 4 and 8 MPa. Based on the experimental results, they developed a correlation for average gas diffusivities as follows:

$$\ln D = d_0 + d_1(T + 273.15) \quad (2.8)$$

Reference	Gas	Bitumen	Diffusivity Correlation
Hayduk & Cheng, 1971	Varity of solvents	11 different solute	$D = \alpha\mu^{-\beta}$
Hiss & Cussler, 1973	-	-	$D = \alpha\mu^{-2/3}$
Hayduk et al., 1973	Propane	Peace River	$D = 0.0591 \times 10^{-9}\,\mu^{-0.545}$ D (m^2/s); μ (Ps)
Hayduk & Minhas, 1982	Propane	Peace River	$D = 13.3 \times 10^{-8} T^{1.47} V_a^{0.71} \mu^{(10.2/V_a - 0.791)}$ D (cm^2/s); μ (cP)
Das and Butler, 1996	Propane	Peace River	$D = 1.306 \times 10^{-9}\,\mu^{-0.46}$ D (m^2/s); μ (Ps)
Das and Butler, 1996	Butane	Peace River	$D = 4.131 \times 10^{-9}\,\mu^{-0.46}$ D (m^2/s); μ (Ps)
Upreti and Mehrotra, 2002	CO_2 CH_4 C_2H_6 N_2	Athabasca bitumen	$\ln D = d_0 + d_1(T + 273.15)$ D (m^2/s)

Table 2.1 Different Correlations for Diffusivity Estimation

Table (2.2) indicates the available diffusivity data of gases in bitumen and heavy oils (Upreti and Mehrotra, 2002)

Boustani and Maini (2001) carried out several experiments in Hele-Shaw to identify the main processes governing the interfacial mass transfer of solvent into bitumen. They compared the predicted intrinsic diffusivity in Panny bitumen as a function of solvent concentration based on three different correlations. They found the estimated diffusivities by Das and Butler (1996) were an order of magnitude higher than those estimated by the Hayduk et al. (1973) and Hayduk and Minhas (1982) correlations. The reason for this discrepancy is that Das and Butler (1996), used α and β coefficient through an optimization procedure that provide a better history match to their experiments in Hele-Shaw cell. In that regard, any additional mechanism that could have affected the experimental rates in Hele-Shaw is overlooked. They found that incorporation of dispersion effects into mass transfer models of Vapex process reduces the discrepancy between the experimental results and analytical models at identical values of Peclet number.

Researchers at the University of Waterloo have measured the viscosity and the density of live oil and the saturation mass fraction of different solvent gases at the vapor/oil interface. These parameters were very important in order to determine the mass transfer coefficient.

Jin et al. (1999) performed vapor extraction experiments to extract Peace River bitumen in a packed column using butane as a solvent. He formulated an empirical correlation between the live oil viscosity μ_0 and butane concentration.

The correlation in terms of butane concentration C_B and viscosity μ_0 in centi poise is given as:

$$\mu_0(C_B) = 16609 C_B^{-2.12} \tag{2.9}$$

The correlation in terms of butane mass fraction X_A in live oil was:

Reference	Bitumen	Gas	Pressure (MPa)	Temperature (°C)	Diffusivity x 10^9 (m^2/s)
Schmidt et al. 1982, 1986	Athabasca bitumen	CO_2	5	20 50 75 100 125 150 175 200	0.28 0.50 0.71 0.92 1.15 1.41 1.55 1.75
Grogan et al. 1988	Maljamar Crude Oil	CO_2	5.2	25	2.1
Denoyelle and Bardon 1984	Stock Tank Oil	CO_2	15	66 75 80	3 8.5-9.2 4.6
Zhang et al. 1998	Heavy Oil	CO_2	2.84	21	4.76
Nguyen and Farouq Ali 1998	Aberfeldy Oil	CO_2	1	23	6
Schmidt et al. 1986	Athabasca bitumen	CH_4	5	50	0.4-0.75
Schmidt et al., 1986	Athabasca bitumen	C_2H_6	5	20 50 75	0.175 0.174 0.337
Upreti and Mehrotra 2000	Athabasca bitumen	CO_2	4	25 50 75 90	0.1335 0.2338 0.3739 0.4280
Upreti and Mehrotra 2000	Athabasca bitumen	CO_2	8	50 75 90	0.3980 0.7436 0.9319
Upreti and Mehrotra 2000	Athabasca bitumen	CH_4	4	25 75 90	0.0810 0.2932 0.4315
Upreti and Mehrotra 2000	Athabasca bitumen	CH_4	8	25 50 75	0.0582 0.1518 0.2029
Upreti and Mehrotra 2000	Athabasca bitumen	N_2	4	25 50 75 90	0.0180 0.0513 0.2335 0.4960
Upreti and Mehrotra 2000	Athabasca bitumen	N_2	8	25 50 75 90	0.0555 0.1717 0.4649 0.7460

Table 2.2 Diffusivity Data of Gases in Bitumen and Heavy Oils

(Upreti and Mehrotra, 2002)

$$\mu_0(X_A) = 0.0094655 X_A^{-2.12} \text{ (g/cm.s)} \quad (2.10)$$

For butane mass fraction in live oil equals to zero, this correlation does not apply.

Oduntan et al. (2001a; 2001b) have developed a new lab scale experimentation method to investigate the effect of various geological factors such as pore structure, heterogeneity of a reservoir on vapor extraction process. Their experiments showed that the accumulation of oil in low permeability zones of layered reservoirs results in lower production rates compared to homogeneous reservoirs of the same average permeability. They used the permeability of 25, 85, 136 and 192 Darcy in their Vapex experiments, and they found that the volumetric flow rate of heavy oil and bitumen produced can be correlated as

$$Q = 0.0348\ K^{0.47} \text{ (cm}^3\text{/min)} \quad (2.11)$$

The overall recovery was found to be about 85 – 92% of the initial oil in place.

The presence of light hydrocarbons (butane and propane) in heavy oil was found to drastically reduce the viscosity.

Table (2.3) indicates some of the live oil properties.

Reference	Bitumen Type	Reservoir Type	Solvent	Viscosity (cP)		Solvent Solubility ω_s
				Bitumen	Live Oil	
Oduntan, 2001	Cold Lake	Homogeneous	Butane	40,550	2-3	0.37
Oduntan, 2001	Cold Lake	Heterogeneous	Butane	40,550	2-3	0.40-0.43
James, 2003	-	Homogeneous	Butane	85,000	2-3	0.27-0.32
Ramakrishnan, 2003	-	Homogeneous	Propane	85,000	4-6	0.35-0.40
Butler & Mokrys (1993)	Tangleflags Oil	Homogeneous	Propane	10,000	2,200 (viscosity of live oil measured on a solvent free basis)	
Butler & Mokrys (1998)	Peace River bitumen	Homogeneous	Propane	126,000	1,900 (viscosity of live oil measured on a solvent free basis)	

Table 2.3 Live Oil Properties

2.2 Dispersion of Solvent Gases in Heavy Oil and Bitumen

Diffusion is a special case of dispersion where the fluid is stationary (convective flow rate is zero). To certain extent, dispersion is identical to diffusion. However, dispersion is a more general term but occurs when macroscopic motion or flow exists.

Dispersion is a combined effect of molecular diffusion, convective motion, Surface renewal, viscosity reduction and gravity drainage. In the extraction of heavy oil and bitumen using vaporized gases, as the gas diffuses into oil, it swells and gets diluted and drains under the action of gravity. While the oil is draining, another surface of heavy oil gets exposed to gas. That is how oil surface renewal takes place (Figure 2.1). Thus, gas diffuses along while oil is moving.

Dispersion in porous media comprises concentration gradients, which are longitudinal and transverse to the direction of oil-solvent flow. These two components of dispersion are thus referred to as longitudinal and transverse dispersion. To date, not much work has been reported on dispersion between high and low viscosity fluids, which results in significant change in solute viscosity (Oballa and Butler, 1989).

Several authors used diffusion and effective diffusion in their mathematical model to predict the production in vapor extraction of heavy oil and bitumen. However, they found that the predicted production was lower than experimental production. Hence, they claimed that dispersion is necessary to predict the actual production rate.

Perkins and Johnston (1963) reported the relationships for longitudinal and transverse dispersion as the sum of diffusion and dispersion terms and the relations were as follows:

$$\frac{K_l}{D_0} = \frac{1}{F\varphi}\left(\begin{matrix}\text{Molecular}\\ \text{Diffusion}\end{matrix}\right) + 0.5\frac{U\sigma d_p}{D_0}\left(\begin{matrix}\text{Convective}\\ \text{Dispersion}\end{matrix}\right); \quad \frac{U\sigma d_p}{D_0}\left(\begin{matrix}\text{Peclet}\\ \text{Number}\end{matrix}\right) < 50 \tag{2.12}$$

$$\frac{K_t}{D_0} = \frac{1}{F\varphi}\left(\begin{matrix}\text{Molecular}\\ \text{Diffusion}\end{matrix}\right) + 0.0157\frac{U\sigma d_p}{D_0}\left(\begin{matrix}\text{Convective}\\ \text{Dispersion}\end{matrix}\right); \quad \frac{U\sigma d_p}{D_0}\left(\begin{matrix}\text{Peclet}\\ \text{Number}\end{matrix}\right) < 10^4 \tag{2.13}$$

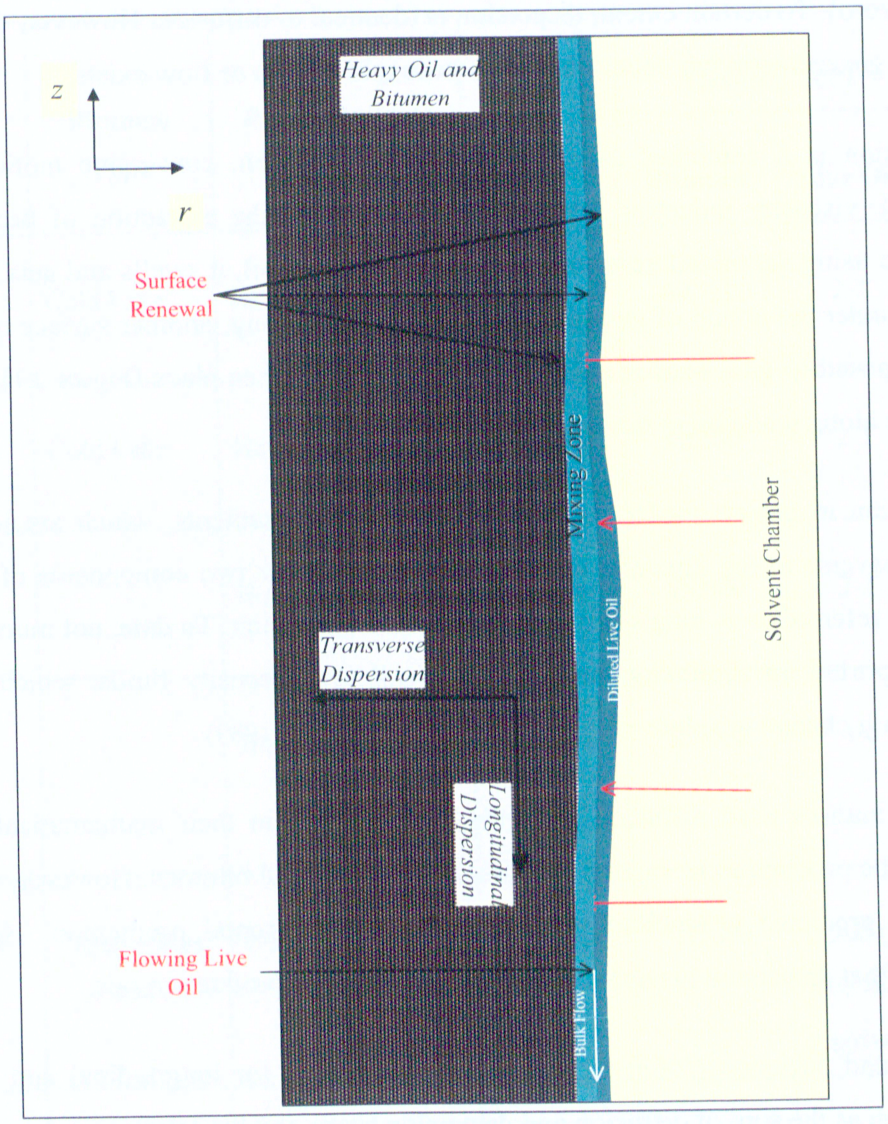

Figure 2.1 Surface renewal in Vapex process

where K_l and K_t are the longitudinal and transverse dispersion coefficient respectively, d_p is the particle diameter, σ is the inhomogenetity factor, D_0 is the molecular diffusion coefficient, U is convective fluid velocity in the direction of bulk flow, F is a formation factor and φ is the porosity of the system.

Dunn et al. (1989) proposed and tested a gravity drainage concept for in situ recovery of bitumen by mobilization with soluble gases at ambient reservoir temperature conditions. Experiments were performed using Carbon dioxide and ethane gases at 20°C to recover Athabasca bitumen from a scaled reservoir model. They modified the thermal gravity drainage for the mass transfer case. They found that the measured drainage rates were higher than those predicted by the model using molecular diffusivity. Thus, to match their experimental results using the theoretical model, they used an effective diffusivity, two to three orders of magnitude higher than the reported molecular diffusivity. They pointed out the possibility of increased recovery due to dispersion. This could not be explained using correlations available for dispersion.

Das and Butler (1994b) examined Vapex with gaseous butane as a solvent, and found that porous media enhanced the rate of heavy oil and bitumen recovery by three to five times. The deasphalting and in situ upgrading of heavy oil and bitumen was found to be less than that with propane as a solvent.

Das (1995) reformulated the earlier mathematical model developed by Butler and Mokrys (1989) to predict the recovery rate, incorporating an apparent diffusion coefficient D_{app} of solvent in bitumen in presence of porous media. He related the intrinsic molecular diffusion D_0 to apparent diffusion coefficient D_{app} in porous media by the following relationship:

$$D_{app} = D_0 \varphi^{\Omega} \tag{2.14}$$

Where Ω is a cementation factor which is a measure of consolidation of rock. For the case of unconsolidated rocks he used 1.3 as a cementation factor, which was originally reported by Pirson (1958). The modified model was as follows:

$$Q = \sqrt{2kg\phi^{\Omega}\Delta S_0 N_S h} \tag{2.15}$$

Where N_S is a dimensionless number given by, which is the function of concentration, density difference, diffusivity and viscosity.

Das and Butler (1998) conducted series of experiments in a sand pack with Peace River and Lloydminster bitumen and butane gas as solvent. They found that experimental production rate was significantly higher than the predicted value from the modified analytical model by Das (1995). They suggested that several factors contributing to recovery rate enhancement in porous media. These factors are: extended interfacial area, increased rate of solubility, capillary action and surface renewal. They realized that the effective diffusion, 3 to 10 times higher than molecular diffusion, is required to match their experimental results with analytical model.

Lim et al. (1996) applied the concept of cyclic stimulation with light hydrocarbon solvent gas through a single horizontal well to recover bitumen from Cold Lake oil sand in three dimensional scaled physical model experiments. They used Ethane gas as a solvent instead of propane because its phase transition properties match Cold Lake reservoir conditions. The experiments showed that the production rate of bitumen assuming a gravity drainage drive mechanism with single horizontal well was significantly higher than that could be expected from the molecular diffusion rate of solvent into bitumen. They had pointed out solvent dispersion as one of the viable processes governing the mass transfer of solvent into bitumen. Based on experimental data and a process model, the effective diffusivity of solvent in heavy oil and bitumen turned out to be two to three orders of magnitude higher than molecular diffusivity.

Nghiem et al. (2001) had modified an equation of state compositional simulator to include the modeling of asphaltene precipitation, molecular diffusion and convective dispersion. The asphaltene precipitate was modeled as a pure solid that flow as a suspension in the oil phase, or deposit onto the rock surface. They performed simulation of a typical Vapex process using Lindbergh oil with propane to study asphaltenes precipitation, and mixing through molecular diffusion and convective dispersion. Their calculated asphaltene

precipitation profiles corresponded to experimental observations. They concluded that the mixing mechanism is effectively controlled through a total dispersion coefficient. They also showed through sensitivity analysis that larger dispersion coefficient result in higher mixing.

Boustani and Maini (2001) studied the role of diffusion and convective dispersion in VAPEX by using a Hele-Shaw Cell, and incorporated the results in a predictive model. The incorporation of dispersion effects into a Vapex mass transfer model at an identical value of Peclet number showed good agreement between theory and experiment. In their work, the overall mass transfer in Vapex process was modeled in 2D space for longitudinal and transverse dispersion. They considered the effect of longitudinal and transverse dispersion due to velocity in x-axis and z-axis respectively as:

$$\frac{K_x}{D_0} = \frac{1}{F\phi} + 0.5\frac{U_x \sigma d_p}{D_0} + 0.0157\frac{U_y \sigma d_p}{D_0} \tag{2.16}$$

$$\frac{K_y}{D_0} = \frac{1}{F\phi} + 0.5\frac{U_y \sigma d_p}{D_0} + 0.0157\frac{U_x \sigma d_p}{D_0} \tag{2.17}$$

Cuthiell et al. (2003) employed a computed Tomography scanner to describe the phenomena of diffusion/dispersion and viscous fingering of liquid toluene solvent in Lloydminster oil dispersed in sand and silica packs at 25°C. The computed Tomography scanner was used to observe details of the liquid solvent distribution in bitumen, as a solvent flood progressed. They also simulated important solvent displacement characteristics with assumed solvent dispersion coefficient. To simulate the viscous instability of solvent displacement, they used a two dimensional spatial grid with alternating porosity. They considered dispersion along vertical direction ten times of that along horizontal direction. Using different values of solvent dispersion coefficients, they also extricated physical dispersion from its numerical counterpart.

Das (2005) investigated the nature of the diffusion boundary layer and solvent distribution. Different values of diffusion and dispersion coefficients in a two

dimensional model were used. He found that in a microscopic nature of the mechanism it is difficult to model the process using a constant value of bulk diffusion coefficient. The concentration-dependence is reasonable because the phenomena such as diffusion and viscosity that are embodied in dispersion are strongly influenced by solvent concentration. He also reported that Vapex process, whether in laboratory model or in the reservoir porous media, takes place in microscopic level.

Kapadia et al. (2006) developed a detailed mathematical model to describe Vapex in a homogeneous porous rectangular block medium, which shrunk with time and space during the vapor extraction process. The model was developed and simulated on the basis of experimental data from Vapex experiments performed by Oduntan (2001). The optimum dispersion of butane as well as its solubility was determined for which the root mean square fractional error between the simulated and experimental values of live oil production was minimum. The concentration-dependent dispersion of butane in Cold Lake bitumen dispersion was determined as

$$D = 5.56 \times 10^{-5} \omega \, (\mathrm{m}^2/\mathrm{s}) \tag{2.18}$$

Where ω is the mass fraction of butane in Cold Lake bitumen.

From the preceding literature review, it appears that dispersion is a viable mechanism for enhanced mass transfer in the extraction of heavy oil and bitumen using vaporized hydrocarbon gases. In spite of this fact, a very little work has been done in this area. In order to assess the role of dispersion of butane gas in heavy oil and bitumen production rates for different permeability media, Vapex experiments in a homogeneous porous cylindrical model saturated with Athabasca bitumen using three different glass beads sizes were performed and will be described on the next chapter.

3 Experimental Set-up and Procedure

This chapter describes the details of the experimental set-up and procedure used to perform vapor extraction of Athabasca bitumen using butane gas as a solvent. Generated experimental data were used to calculate the live oil viscosity, density, cumulative production rate, and the solubility of butane gas in Athabasca bitumen. This chapter will also include details of permeability determination for different physical models packing.

3.1 Experimental Set-up

The schematic of the experimental set up used in this work is shown in Figure (3.1). This set up was used to perform Vapex experiments in order to determine the dispersion coefficient of butane gas into the heavy oil and bitumen.

Oil-saturated porous medium with glass beads of known permeability was packed in a cylindrical wire mesh of 21 cm height, and 6 cm diameter (Figure 3.2), and placed inside a transparent poly vinyl chloride (PVC) cylinder. The oil packing was prepared using a known mass of oil, which was placed inside an Incubator [a shaker with temperature controller] at 60°C and 250 rpm. The glass beads were gradually added to the heated oil inside the incubator to ensure proper mixing of bitumen and glass beads without trapping air bubbles. The saturated mixture of heavy oil and glass beads was packed into the cylindrical wire mesh, which was placed inside an ice bath to prevent the oil from oozing out of the mesh. After the entire mesh was packed, it was left at room temperature for one day to reach thermal equilibrium prior to the experiments (Figure 3.3).

The picture of the experimental set up is shown in Figure (3.4). The set up comprises a 15 cm diameter cylindrical pressure vessel of height 162 cm. The physical model was hanged on a load cell inside the pressure vessel. The load cell was used to record the decrease in the mass of the cylindrical packing with time as the oil diluted by the dispersed solvent vapor drained away by the action of gravity.

A small funnel was placed at the bottom of the pressure vessel to collect the drained oil

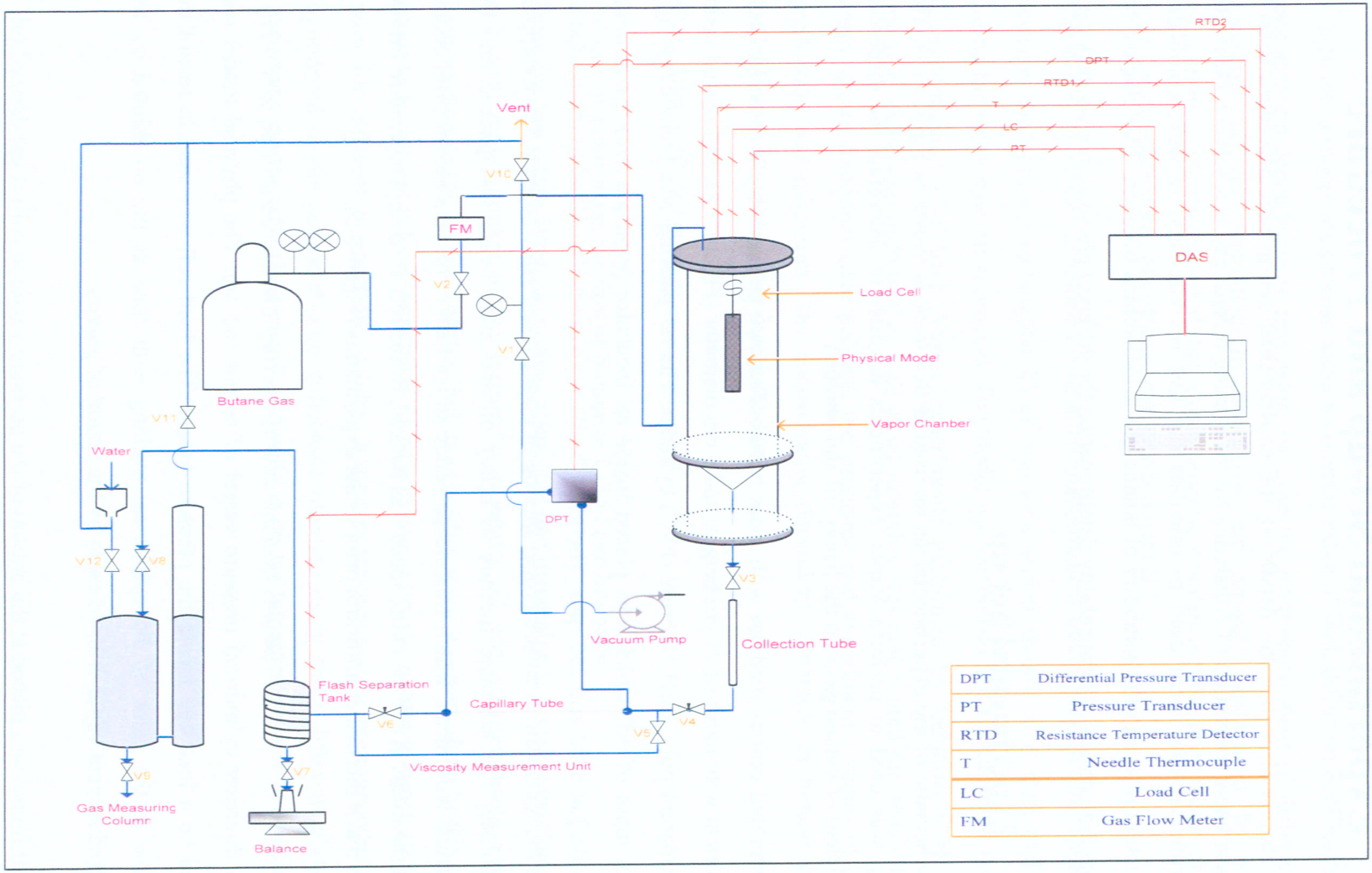

Figure 3.1 Schematic Diagram of Experimental Setup

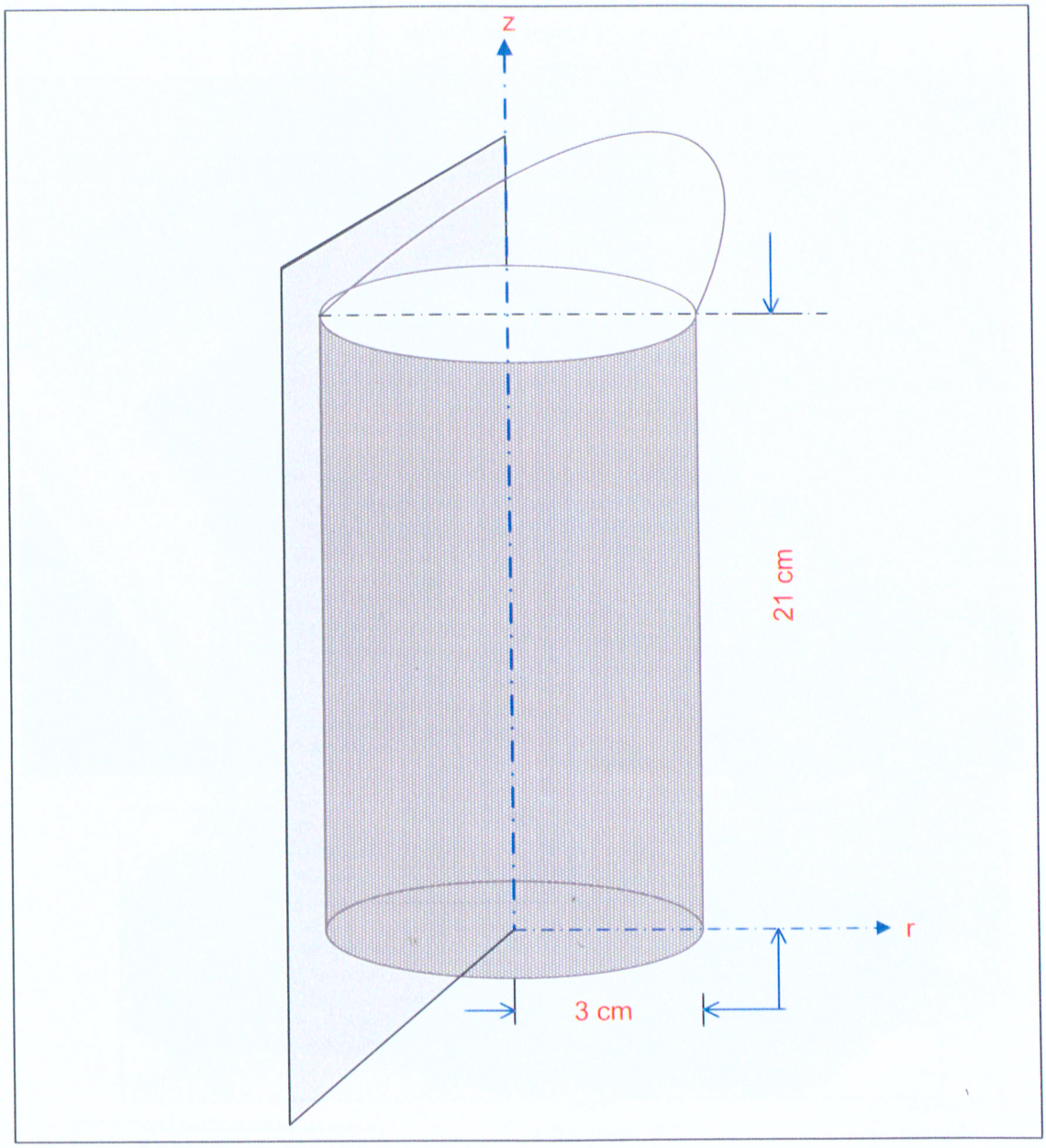

Figure 3.2 Schematic diagram of the Physical Model

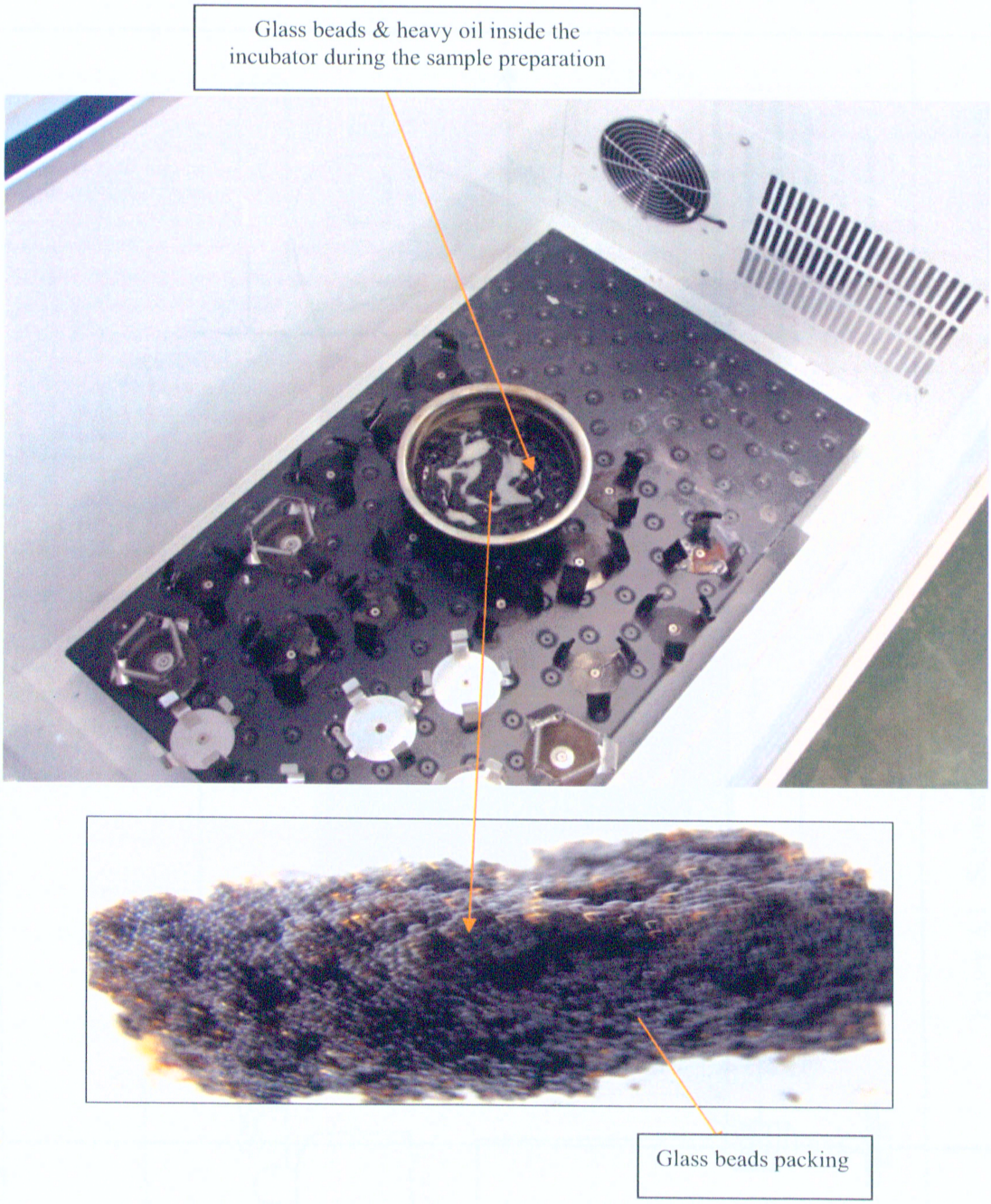

Figure 3.3 Picture of the Glass Beads Packing

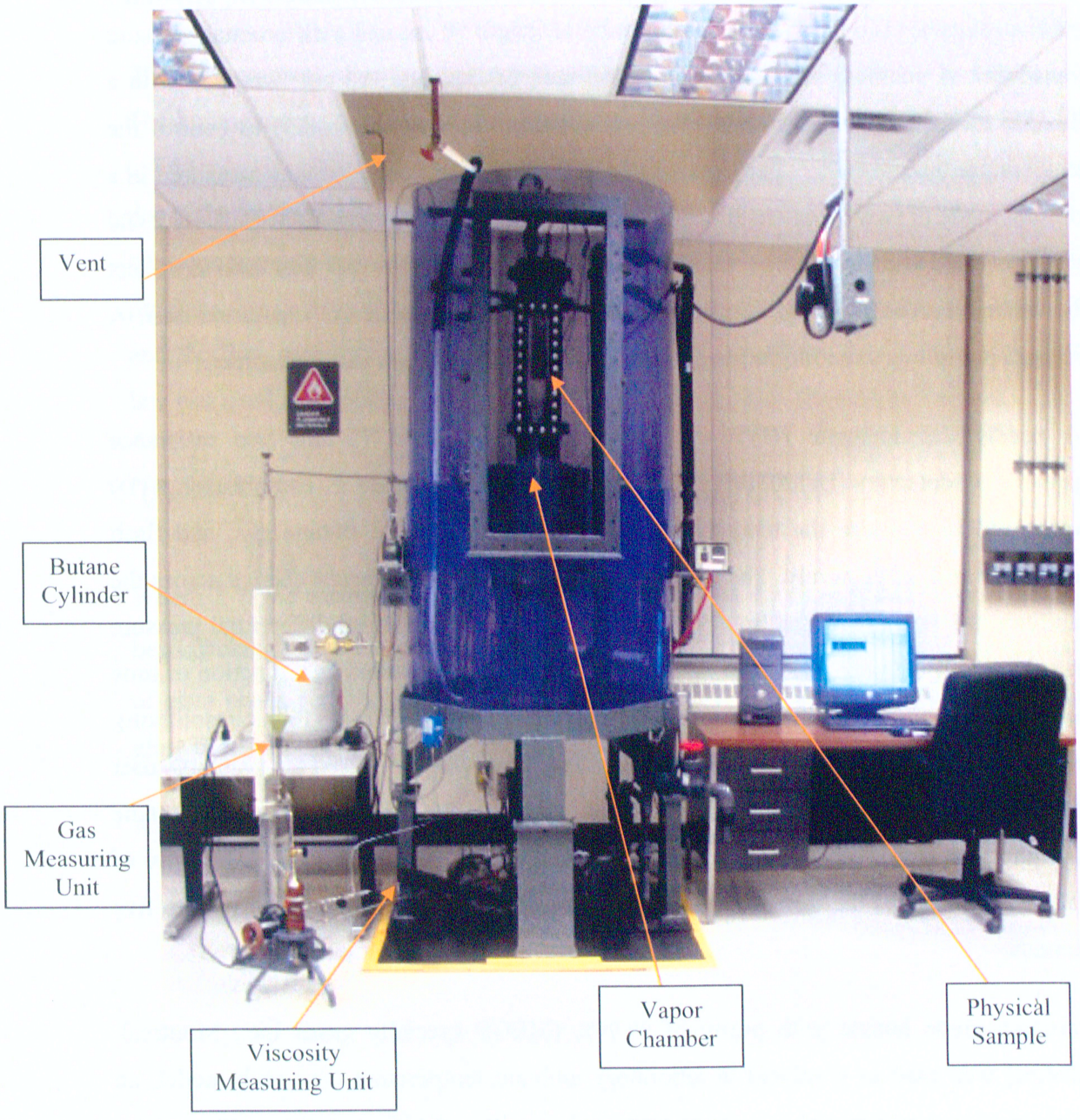

Figure 3.4 Picture of the Experimental Setup

and direct it to a calibrated 25 cm^3 collection tube.

The tube was connected to a viscosity measurement unit comprising of a 0.1016 cm internal diameter stainless steel capillary tube of length 50 cm and a differential pressure transducer. A stainless steel flash separation tank of capacity 300 cm^3 wrapped with a flexible electrical heating tape (HTWC101, heating tape with controller) to control the temperature around 60°C. The volume of the gas from the flash tank was measured in a column made of two cylinders attached to each other. The first cylinder of capacity 2,600 cm^3 was filled with water. The second cylinder of capacity 2,900 cm^3 was used to collect the water removed from the first one when butane flashed out of the separation tank. A vacuum pump was used for purging. The whole setup rested on a shock absorber.

A needle thermocouple (HYP1-30, autoclave probe; Type T) and two resistance temperature detectors (E11202108, high pressure RTD sensor and CF, compression RTD) were used to measure the temperature of the physical sample, butane gas, and flash separation tank respectively. The butane gas pressure and the pressure change across the capillary tube were recorded by a pressure transducer and industrial differential pressure transducer respectively. The experimental conditions were recorded as a function of time automatically by using Ethernet Data Acquisition System – EDAS (16 bit resolution), which was connected with the computer. Labview 7 software was used for graphical user interface and online monitoring of following inputs: (i) the temperatures of the butane gas, physical, and flash separation tank, (ii) pressure of butane gas, (iii) inlet flow of butane gas, and (iv) the mass of the physical sample. The sampling time was set to five seconds.

Research grade butane with purity of 99.99% (MEGS specialty gases Inc., Montreal, Quebec) was used as a solvent at laboratory ambient temperature. For each model, an experiment was conducted at a room temperature with ± 0.5 °C variation, and pressure close to butane dew point with variation ± 0.007 MPa. Although the desirable solvent for Vapex process is propane because of its higher diffusivity (Das and Butler, 1996) utilization of butane rather than propane is due to limitation of the working pressure of the transparent PVC pressure vessel that acts as a vapor chamber.

Knowing the density and mass of the heavy oil and glass beads, the porosity of the physical model was determined to be 0.38. Three different sizes of glass beads with different permeability's were used to pack homogeneous physical models.

The measurement of permeability was carried out with apparatus shown in Figure (3.5). The homogeneous packing of glass beads and heavy oil was prepared inside a gray PVC cylinder having same cavity as the physical model (21cm x 6cm). Once the packing was done, the packing was tested for permeability with respect to air. Air was injected at constant pressure into upper end of the cylinder and exhausted from the lower end. The pressure drop across the cylinder was measured using a differential pressure transducer and the flow rate was measured by flow meter. For one phase steady state flow, Darcy law was used to calculate the permeability of the glass beads packing as follows:

$$Q = \frac{kA}{\mu}\frac{\Delta p}{\Delta L} \tag{3.1}$$

Where k is the permeability, Q is the air flow rate, A is the cross section area of the glass bead packing, μ is the viscosity of the air, Δp is the pressure drop and ΔL is the length of glass beads packing. Figure (3.6) shows the permeability values measured for different glass beads sizes.

A sample of permeability calculations is presented in Appendix A.

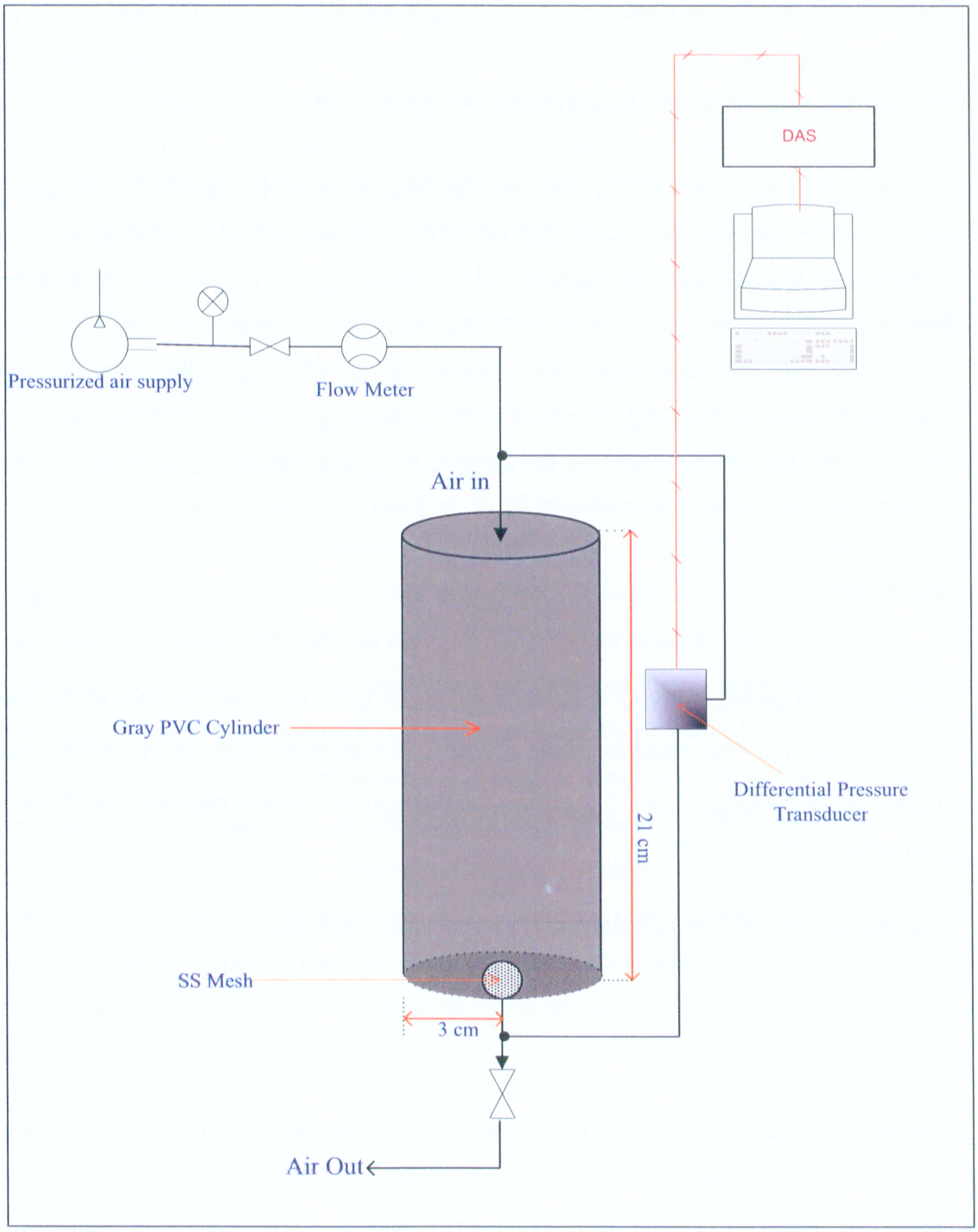

Figure 3.5 Schematic Diagram for Permeability Measurement Apparatus

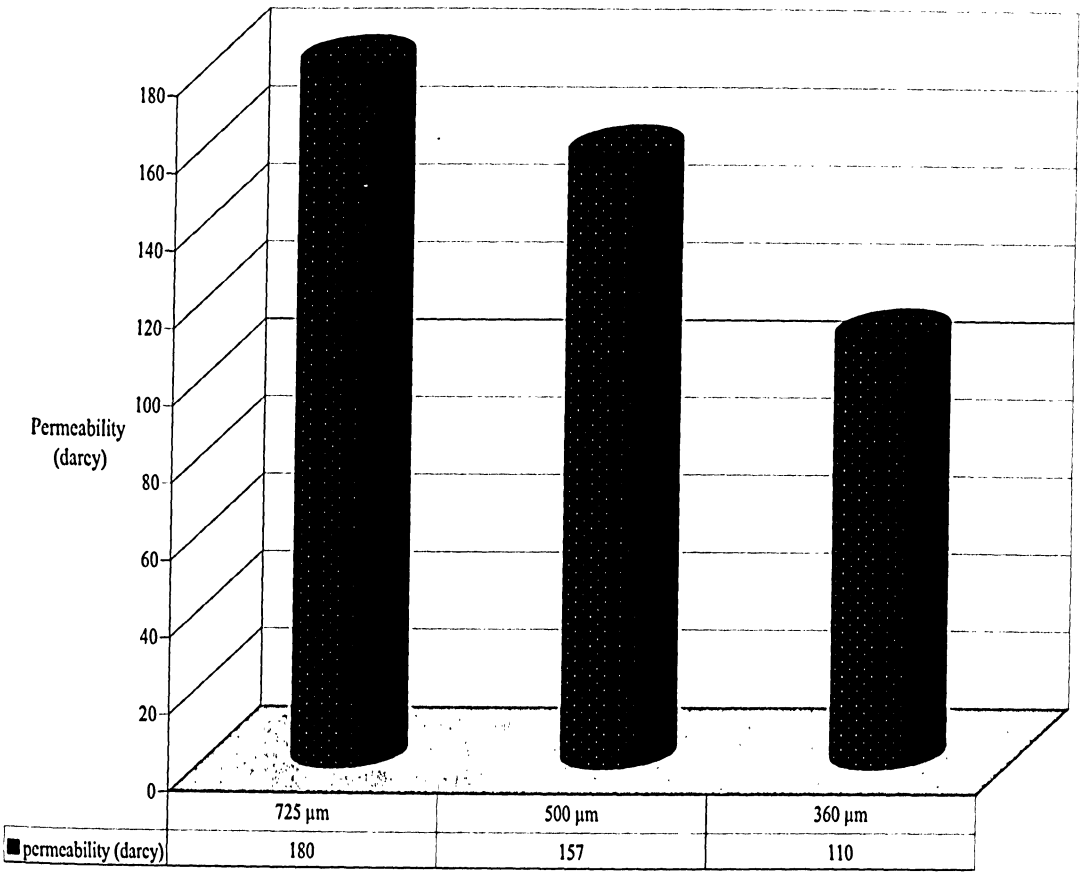

Figure 3.6 Permeability of the Three Different Glass Beads Sizes

3.2 Experimental Procedure

Before each experiment started, the whole experimental setup was pressurized with air and leak-tested. No air leak was detected by the pressure transducer for 12 hours. The cylindrical physical model packed with heavy oil saturated homogeneous porous medium was vertically hanged inside the PVC cylinder. Air was purged from the entire setup by applying -15 mmHg vacuum using a vacuum pump. To ensure complete displacement of dead air, the entire system was flushed with sufficient amount of butane. For flushing a butane gas volume of about twice the void volume of the vapor chamber was pumped from the top port through valve V2 for 15 minutes and exit from the exhaust vent V10. The flush time for one volume was determined by dividing the void volume of the vapor chamber by the gas flow rate. After flushing the whole system with butane, vacuum was applied again until the pressure transducer inside the vapor chamber read -15 mmHg.

After that, a constant supply of butane gas was injected from the top port of the vapor chamber. The vapor chamber and the collection tube were pressurized to delivery pressure of butane in the cylinder, i.e. butane vapor pressure at 1- 2° C below the chamber temperature. A mass flow meter was placed on the supply line to determine the volumetric uptake of the butane into the vapor chamber. In the beginning of the experiment the volumetric flow rate of the gas was 2 L/min and the pressure inside the vapor chamber was -15 mmHg. The pressure gradually builds up and approached the desired value and after that the flow of the gas started to decrease until it reached a constant value of 0.2 L/min. After exposing the physical model to butane for a few minutes, the butane gas diffused into heavy oil, and the surface of the packing absorbed the butane and consequently diluted. The diluted oil had a much lower viscosity and can freely drain under the action of gravity, resulting in live oil production. As the diluted oil drained under gravity new pores filled with heavy oil were exposed into the gas and butane absorption continued to occur until the production was stopped.

A load cell was recorded the decrease in the mass of the physical model as a function of time every 1 minute as the production continued. The produced oil was collected in a

graduated collection tube for measurement of viscosity and flow rate. When about 15 cm^3 of live oil was collected, the oil was drained through a capillary tube into a cylindrical stainless steel flash separation tank. This was accomplished by opening valves V3, V4, V6, V8, and V11 while V5, V7, V9, and V12 were closed (Figure 3.1). A bypass line equipped with a valve V5 was set up to facilitate flow in the event that the capillary tube became plugged. The flash separation tank was wrapped with a flexible heating tape with temperature controller to maintain the temperature inside the separator at 60°C or higher. The librated butane was allowed to enter a graduated gas measuring column from the port located on the top valve V8. The gas measuring column was initially filled with water. The librated volume of butane gas was determined by calculating the volume of the space occupied by the removed water. The produced butane gas free oil "dead oil" amount was collected in a baker placed on a weighing balance after each flashing by opening valve V7.

After production had ceased, the main valves on the butane cylinder were shut and the system depressurized by venting off the butane in the enclosing pipe into the fume hood. Then air was used to push the remaining gas in the vapor chamber to the vent. The model then was taken out of the vapor chamber and weighted. Knowing the model weight before and after commencement of experiment enables the determination the overall oil recovery as a percentage of the original oil in place.

3.3 Live Oil Viscosity Measurement

To determine live oil viscosity online the following experimental procedure was implemented as shown in (Figure 3.7):

A known volume of live oil was collected in the collection tube. The collected live oil was allowed to flow through the attached capillary tube by opening valves V3, V4, and V6 and closing valves V5, and V7. A differential pressure transducer recorded the pressure drop across the capillary for a given flow rate. A needle valve V6 was used to maintain a constant pressure drop across the capillary tube. The flow rate of the live oil was determined by measuring amount of time required to drain a known volume of diluted oil from the collection tube at constant pressure drop.

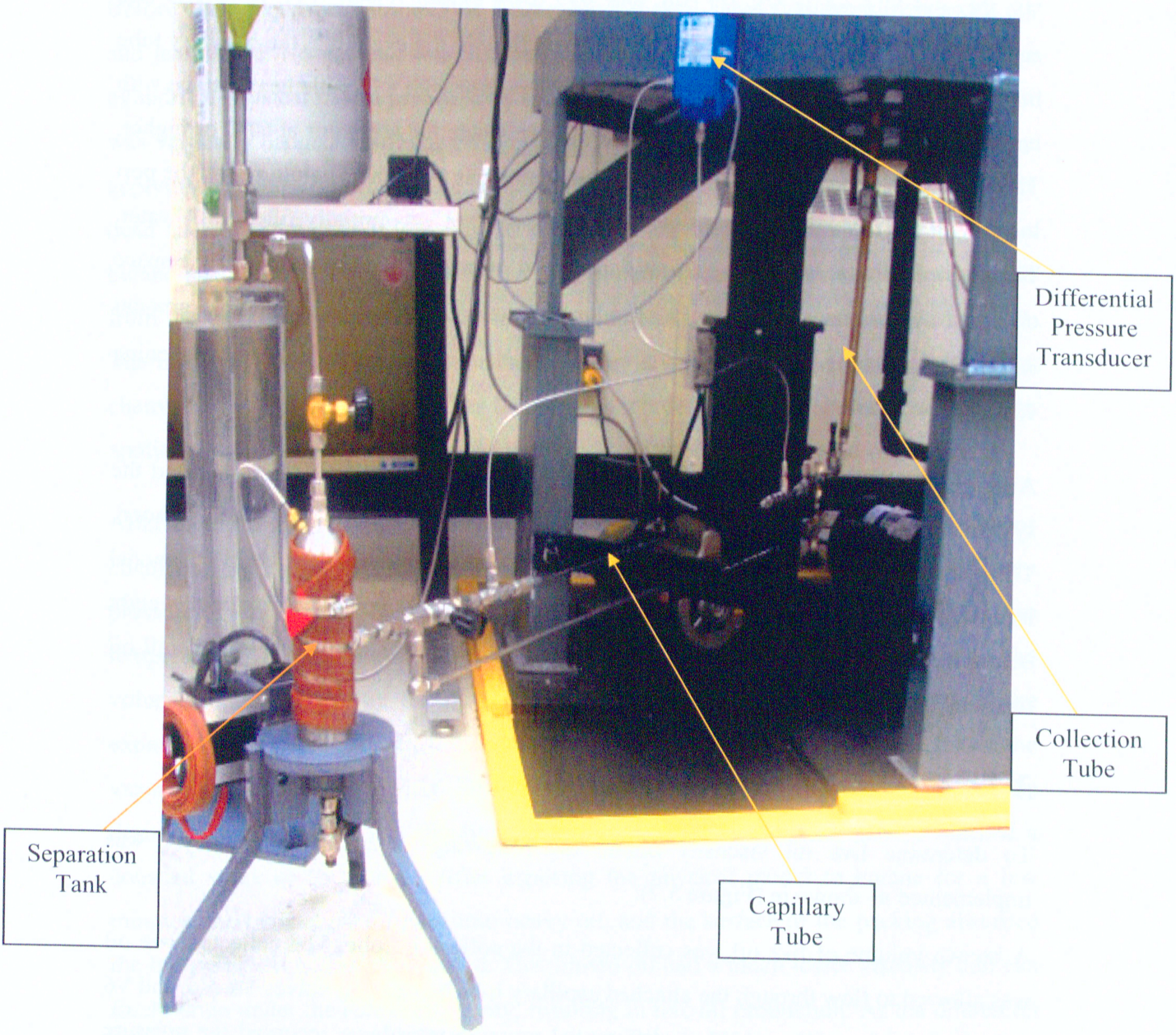

Figure 3.7 Picture of the Viscosity Measuring Unit

Knowing the live oil flow rate "Q", length "L" and diameter "D" of the capillary tube, the pressure drop across capillary tube "ΔP" the viscosity of the live oil was determined from the Hagen – Poiseuille equation:

$$Q = \frac{\pi d^4 \Delta P}{128 \mu L} \tag{3.2}$$

A sample of live oil viscosity calculation is presented in Appendix B

3.4 Butane Gas Solubility Measurement

To determine butane gas solubility the following experimental procedure was implemented:

The live oil was passed through the capillary tube into a flash separation tank. The flash separation tank was wrapped with a flexible heating tape with temperature controller to maintain the temperature inside the separator at 60°C or higher to ensure effective flashing of dissolved butane from the live oil being produced. The live oil was left for a long time in the heated flash tank to ensure that most of the solvent was vaporized.

The librated butane was allowed to enter a graduated gas measuring column from the port located on the top valve V8. The gas measuring column was initially filled with water. The librated volume of butane gas was determined by calculating the volume of the space occupied by the removed water. When most of the water was removed, valve V12 was opened to balance the water level inside the column again; and the column becomes ready for another batch of measurement of produced gas.

Knowing the weight of librated C_4H_{10}, the dead oil weight and the volume of the live oil, the solubility of butane was determined of as well as live oil density by using the following formulas

$$C_4H_{10}\ \text{Dissolved weight fraction} = \frac{\text{weight of librated } C_4H_{10}}{\text{weight of dead oil} + \text{weight of librated } C_4H_{10}} \tag{3.3}$$

$$\text{Live Oil Density} = \frac{\text{weight of librated } C_4H_{10} + \text{weight of dead oil}}{\text{volume of Live Oil}} \quad (3.4)$$

A sample of butane solubility and live oil density calculations is presented in Appendix C.

3.5 Live Oil Production Rates

Production rates of the live oil were measured every five seconds by a load cell. The physical model was hanged on the load cell inside the vapor chamber. The load cell recorded the decrease in the mass of the physical model with time as the oil diluted by the dispersed solvent vapor drained away by the action of gravity. Figure (3.8) shows cumulative production histories for the various permeability packing.

The accuracy of the load cell readings was determined experimentally for different hours during the day. A known solid weight was hanged on the load cell inside the vapor chamber and air was pumped at pressure 0.21 MPa. The readings each time was recorded for 12 hours. The outcomes of these tests were: the load cell is very sensitive to vibration. The standard deviation of the load cell reading was found to be 1.1×10^{-1} during the day time and 9.8×10^{-5} during the night. All the experiments on the thesis were conducted at night.

A sample of cumulative live oil production is presented in Appendix D.

Figure (3.9) shows a comparison of the average production rates for different glass bead sizes. The average production rates were calculated based on the cumulative live oil production divided by total production time during experiment. The production rate was correlated with the permeability of the homogeneous model at dip angle 90° by the following power law relation:

$$\dot{m} = 0.0296\, K^{0.4851} \quad \text{(g/min)} \quad (3.5)$$

where K has units of Darcy

The power law dependency of the production rate with permeability was obtained as shown in Figure (3.10).

The oil recovered was about 88 to 92% by weight from the total oil in place and it was calculated based on the weight of the physical model before an after each run. In all experiments there was no significant production from the last 4cm section at the production end due to the effect of capillarity as observed earlier by the researchers at University of Waterloo.

This laboratory scale physical model of Athabasca bitumen saturated porous medium is used in the following chapter for developing a mathematical model to determine solvent dispersion coefficient in vapor extraction of heavy oil and bitumen process. The experimental data of live oil production generated will be used in the simulation of the model.

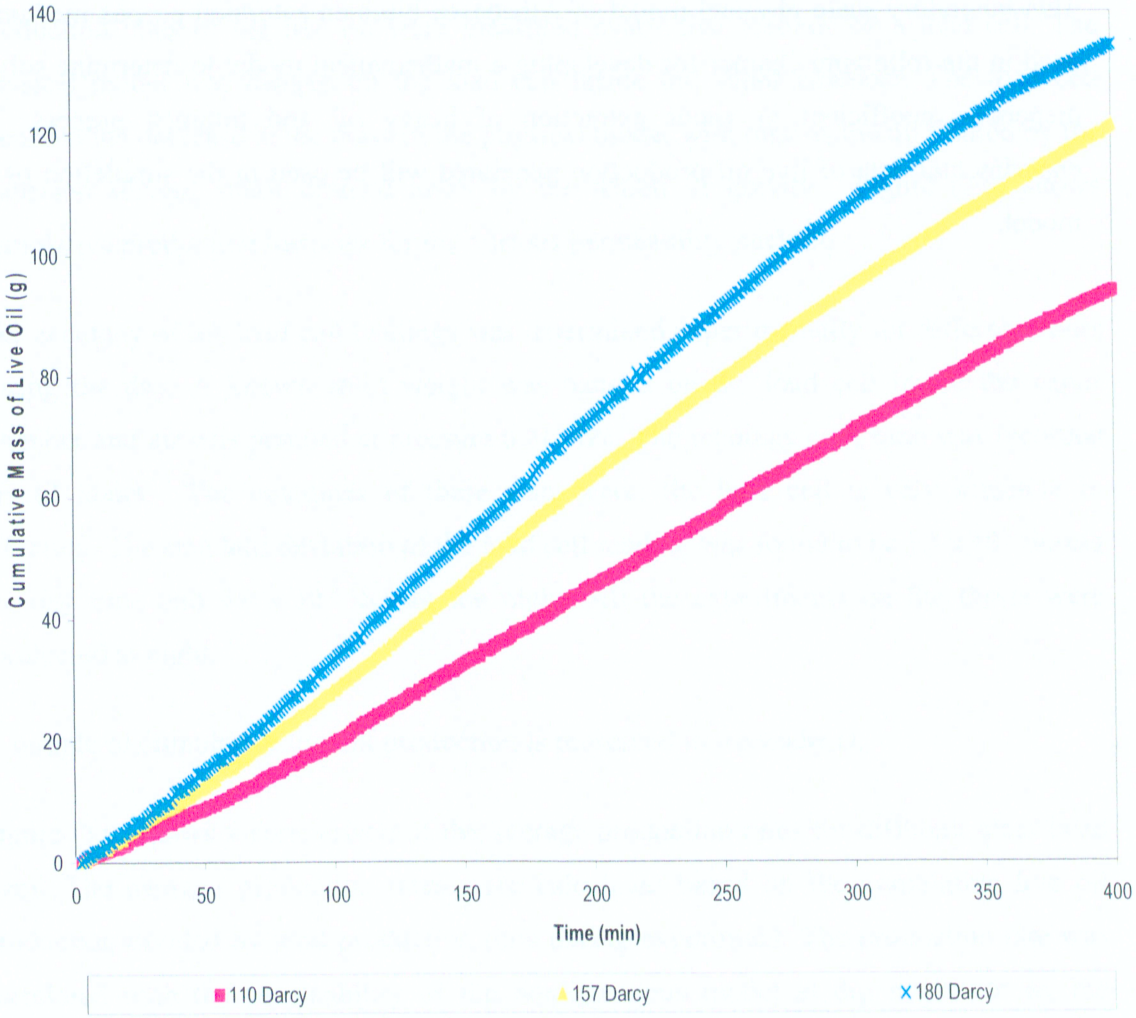

Figure 3.8 Cumulative Live Oil Production for Homogeneous Packing versus Time

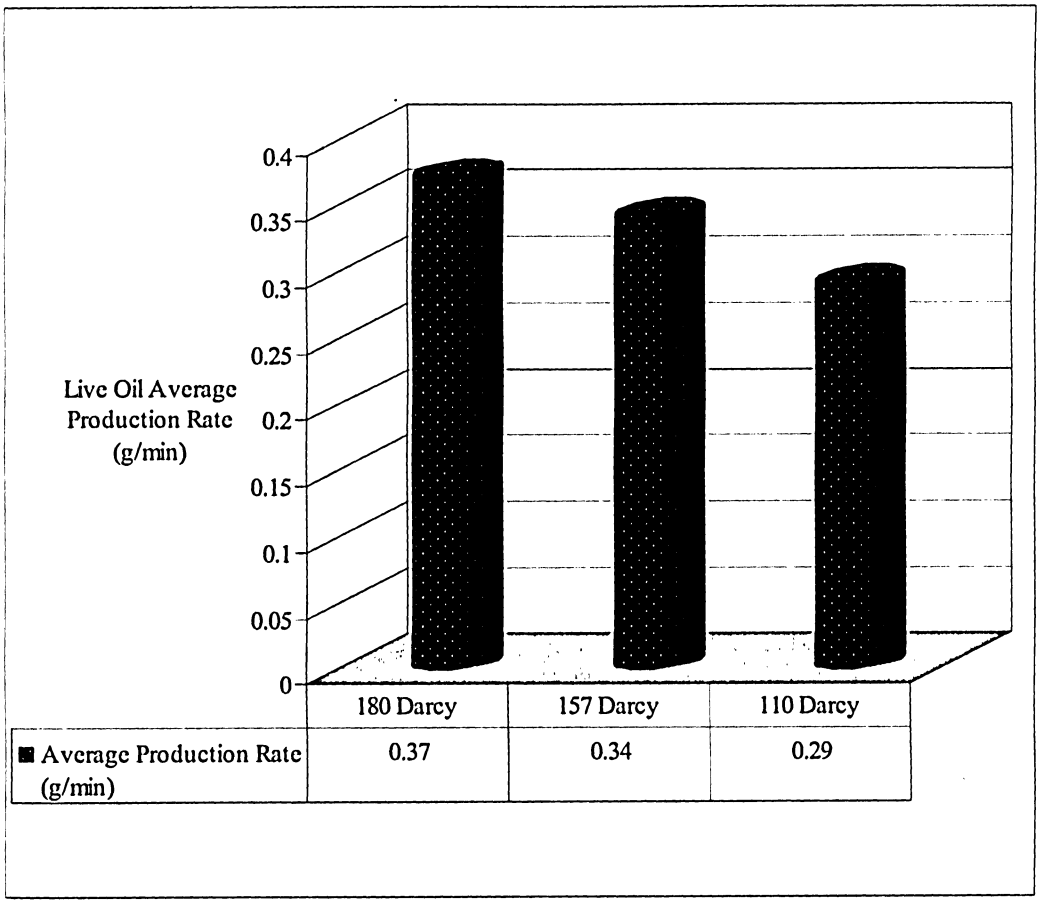

Figure 3.9 Live Oil Production Rates for Different Permeability Packing

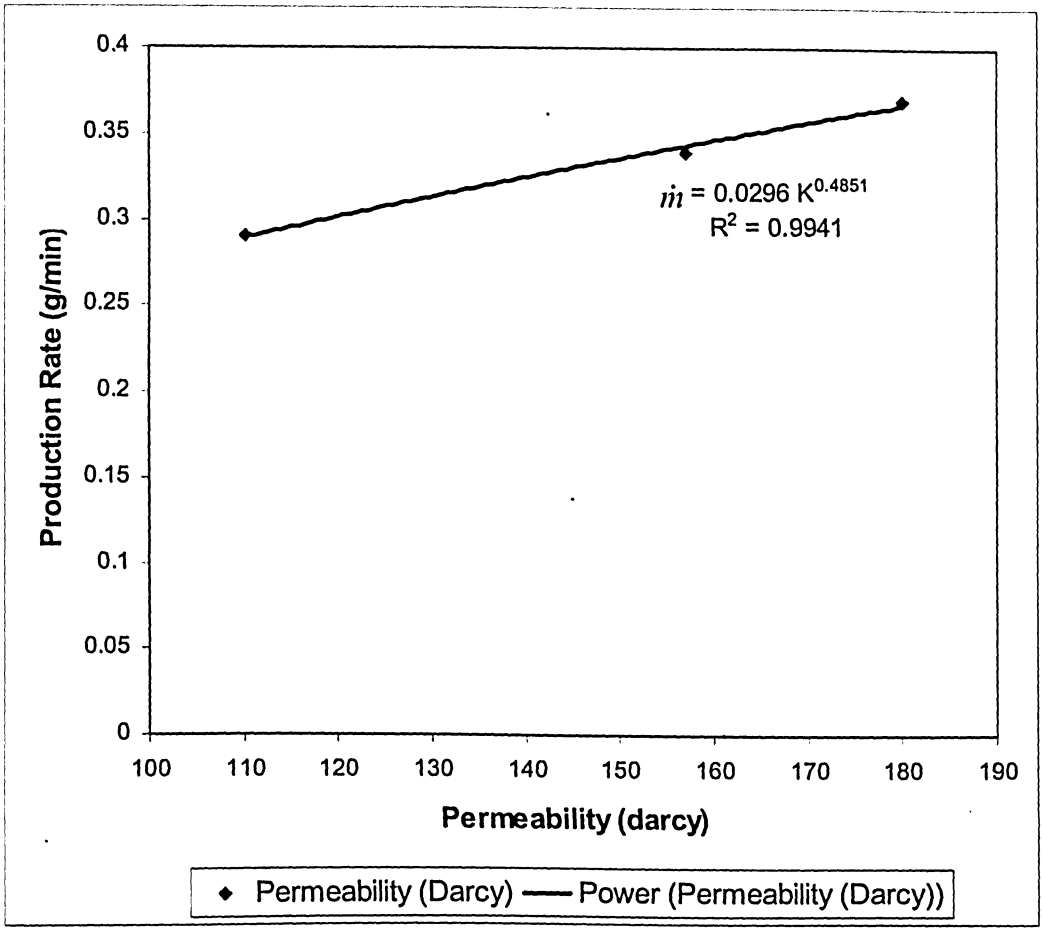

Figure 3.10 Production Rates versus Permeability

4 Mathematical Model

This chapter will present a brief introduction about analytical analysis of dispersion in porous media; development and simulation of a detailed mathematical model to determine the dispersion coefficient of butane gas in Athabasca bitumen for three different permeability packing. This model will be developed based on the vapor extraction experiments conducted in a laboratory scale model as described in previous chapter. Furthermore, the methodology of the mathematical model simulation will be described.

4.1 Introduction

The analysis of fluid flow in porous media has evolved throughout the years along two fronts—the experimental and the analytical. Physicists, engineers, hydrologists, and the like have examined experimentally the behavior of various fluids as they flow through porous media ranging from sand packs to fused Pyrex glass. Based on their analyses, they have attempted to formulate laws and correlations that can then be utilized to make analytical predictions for similar systems.

The mathematical forms of the relationships, which are designed to describe the flow behavior of the reservoir fluids, will vary depending upon the characteristics of the reservoir. The primary reservoir characteristics that must be considered include types of fluids in the reservoir, flow regimes, reservoir geometry, and number of flowing fluids in the reservoir (Bear, 1972)

Mixing at a core scale can be called a microscopic dispersion, and at a reservoir scale can be called a macroscopic dispersion. At a macroscopic scale, this convective transport in a porous media is described by Darcy law. The variation in the reservoir properties results in a macroscopic dispersion. When the fluids are moving through a porous media, the effective diffusion coefficient increases due to convective mixing and the dispersion may be higher than that due to diffusion alone (Perkins and Johnston, 1963).

The difference between theory and experiment is due to enhanced mixing not included in previous theories. The enhanced mixing of the fluid produces an effective diffusion coefficient that largely suppresses gradients in the concentration field, resulting in single-fluid like behavior.

The objective of this chapter is to find dispersion coefficient for butane gas in Athabasca heavy oil, which, when incorporated into the mass transfer model of the experimental dispersion process, would yield a calculated mass of gas dispersed in heavy oil equal to its experimental value obtained practically. The optimal dispersion coefficient of the butane gas is calculated as a function of its concentration in heavy oil. For optimal dispersion coefficient values, the root mean squared relative error between the calculated and the experimental gas mass dispersed in heavy oil and bitumen is minimized.

4.2 Mathematical Model Formulation

A mathematical model is developed below to describe the mass transfer process in the aforementioned experiments. The assumptions of the model developed are as follows:

1. Experiments were carried out at constant temperature (± 0.5 °C) and pressure (± 0.007 MPa).
2. The mass fraction of solvent gas at the exposed surface of porous medium is the saturation mass fraction under equilibrium.
3. The diffusion of the butane gas takes place along the radial direction only.
4. The production of live oil along the radial direction is under influence of molecular diffusion, the effects of surface renewal, viscosity reduction, and capillary action.
5. The flow of the live oil along the vertical direction inside the pores in the boundary layer is governed by the Darcy flow in porous medium.

6. Live oil has constant mass density.

7. Uniform porosity & permeability.

8. There are no chemical reactions as the absorption of the solvent gas in bitumen is purely a physical phenomenon.

The unsteady state mass balance for solvent gas in a cylindrical differential element Figure (4.1) is given by:

$$\begin{pmatrix}\text{Accumulation of the}\\ \text{solvent mass over a}\\ \text{finite time interval } \Delta t\end{pmatrix} = \begin{pmatrix}\text{Rate of the solvent}\\ \text{mass input along}\\ \text{r and z -direction}\end{pmatrix} - \begin{pmatrix}\text{Rate of the solvent}\\ \text{mass output along}\\ \text{r and z -direction}\end{pmatrix} \tag{4.1}$$

As per our assumptions, diffusion of the gas takes place along r-direction (transverse dispersion). The transport of the gas along r-direction is defined by Fick first law

$$\begin{pmatrix}\text{Rate of the solvent}\\ \text{mass input along}\\ \text{r-direction}\end{pmatrix} - \begin{pmatrix}\text{Rate of the solvent}\\ \text{mass output along}\\ \text{r-direction}\end{pmatrix} = \left(J_g S\right)_r - \left(J_g S\right)_{r+dr} \tag{4.2}$$

Where the mass flux of the gas species is given by:

$$J_g = -\rho D \frac{\partial \omega}{\partial r} \tag{4.3}$$

The transfer of the live oil along z-direction is governed by the Darcy flow.

Diffusion of the gas along z-direction is negligible while bulk is moving

$$\begin{pmatrix}\text{Rate of the solvent}\\ \text{mass input along}\\ \text{z-direction}\end{pmatrix} - \begin{pmatrix}\text{Rate of the solvent}\\ \text{mass outputalong}\\ \text{z-direction}\end{pmatrix} = \left(vA\rho\omega\right)_z - \left(vA\rho\omega\right)_{z+dz} \tag{4.4}$$

Substituting equations (4.2) and (4.4) into (4.1) results in the following unsteady state mass balance for solvent gas equation

$$\frac{\partial}{\partial t}\left[V\phi\rho\omega\right] = \left[\left(vA\rho\omega\right)_z + \left(J_g S\right)_r\right] - \left[\left(vA\rho\omega\right)_{z+dz} + \left(J_g S\right)_{r+dr}\right] \tag{4.5}$$

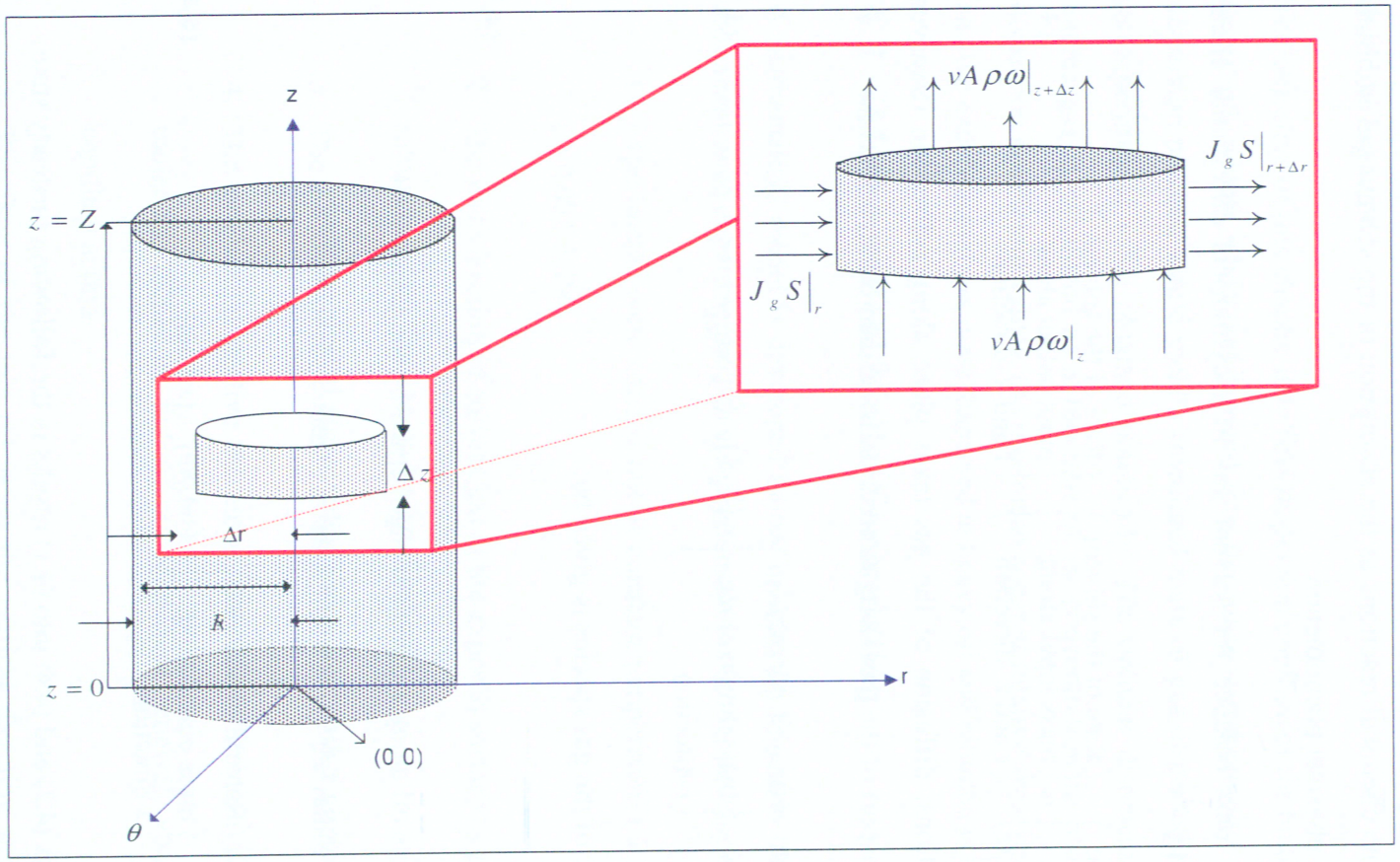

Figure 4.1 Mathematical model Formulation

In equation (4.5), V is finite differential volume, S is finite differential surface area along r-direction and A is finite differential cross-sectional area along z-direction are given by

$$V = 2\pi r dr dz; \qquad S = 2\pi r dz; \qquad A = 2\pi r dr \tag{4.6}$$

Substituting equations (4.3), (4.6) into (4.5) yields in the following unsteady state partial differential equation:

$$\frac{\partial \omega}{\partial t} = -\frac{v}{\varphi}\left(\frac{\partial \omega}{\partial z}\right) + \frac{D}{\varphi}\left(\frac{1}{r}\frac{\partial \omega}{\partial r}\right) + \frac{D}{\varphi}\left(\frac{\partial^2 \omega}{\partial r^2}\right) + \frac{1}{\varphi}\left(\frac{\partial D}{\partial \omega}\right)\left(\frac{\partial \omega}{\partial r}\right)^2 \tag{4.7}$$

In equation (4.7), ω is the mass fraction of the gas, D is the dispersion of the solvent gas along z-direction and v is the Darcy velocity correlation along z-direction given by:

$$v = \frac{K_r K \rho g \cos\theta}{\mu} \tag{4.8}$$

In equation (4.8) μ is the concentration – dependent viscosity of live oil given by the following correlation (Oduntan, 2001)

$$\mu = \mu_0 \omega^{-2} \tag{4.9}$$

For the dispersion of gas in heavy oil and bitumen, the following correlation was used (Das and Butler, 1996)

$$D \propto \mu^{-0.5} \tag{4.10}$$

The change in the height of the bitumen in the physical sample (Z) with time at any location on the r-axis is given by the negative of Darcy velocity

$$\frac{\partial Z}{\partial t} = -v_0 \tag{4.11}$$

where v_0 the negative of Darcy velocity corresponding to the average of live oil velocity over the finite differential volume, $2\pi r$drdz at the bottom, i.e. at $z = 0$.

Initially there was no gas inside the packing. However, at all time, its surface has the solvent gas concentration equal to its equilibrium saturation concentration under

prevailing temperature and pressure. There is no production of the live oil at the beginning so that the initial height of the bitumen sample is Z_0.

Thus the initial conditions at t = 0 are

$$\omega = \begin{cases} 0, & \forall\ 0 \le z \le Z, \quad \forall\ 0 \le r < R \\ \omega_{sat} & \forall\ 0 \le z \le Z, \quad r = R \end{cases} \tag{4.12}$$

$$Z = Z_0 \qquad \forall\ 0 \le r < R$$

At all times, the entire exposed circumference and the top face of the cylinder was saturated with gas. There is no mass transfer at the bottom of the cylinder

Thus the boundary conditions at t ≥ 0 are

$$\omega = \omega_{sat} \begin{cases} \forall\ 0 \le z \le Z, & r = R \\ \forall\ 0 \le r < R, & z = Z \end{cases} \tag{4.13}$$

Due to symmetry, for all z,

$$\frac{\partial \omega}{\partial r} = 0; \quad 0 \le z \le Z \text{ and } r = 0 \tag{4.14}$$

The cumulative mass of produced live oil at any time is given by

$$m_{cal} = 2\pi\rho \int_0^R (Z_0 - Z)\, r dr \tag{4.15}$$

4.3 Mathematical Model Solution

The mathematical model was numerically solved using finite difference method. Application of second order finite difference along r and z-directions results in the set of simultaneous ordinary differential equations with time as an independent variable. N_i and N_j grid points respectively along r and z-directions.

The finite difference ordinary differential equations are as follows:

➢ For intermediate grid points in the cylinder:

$$\frac{d\omega_{i,j}}{dt} = -\frac{K_r K \rho g \cos\theta}{\mu_0 \varphi}(\omega_{i,j})^2\left(\frac{\omega_{i,j+1}-\omega_{i,j-1}}{z_i}\right) + \frac{D_0}{\varphi}\left(\frac{\omega_{i+1,j}-\omega_{i-1,j}}{(\Delta r)^2}\right)^2 + \frac{D_0\omega_{i,j}}{\varphi}\left(\left(\frac{1}{r_i}\frac{\omega_{i+1,j}-\omega_{i-1,j}}{(\Delta r)^2}\right)+\left(\frac{\omega_{i+1,j}-2\omega_{i,j}+\omega_{i-1,j}}{(\Delta r)^2}\right)\right) \tag{4.16}$$

$0 < i < N_i - 1$ *and* $0 < j < N_j - 1$

➢ For all grid points on the center, except endpoints

$$\frac{d\omega_{0,j}}{dt} = -\frac{K_r K \rho g \cos\theta}{\mu_0 \varphi}\omega_{0,j}^2\left(\frac{\omega_{0,j+1}-\omega_{0,j-1}}{z_0}\right); \qquad 0 < j < N_j - 1 \tag{4.17}$$

➢ For the bottom corner grid point on the centre

$$\frac{d\omega_{0,0}}{dt} = -\frac{K_r K \rho g \cos\theta}{\mu_0 \varphi}\omega_{0,0}^2\left(\frac{\omega_{0,1}-\omega_{sat}}{z_0}\right) \tag{4.18}$$

➢ For the upper corner grid point on the centre

$$\frac{d\omega_{0,N_j-1}}{dt} = -\frac{K_r K \rho g \cos\theta}{\mu_0 \varphi}\omega_{0,N_j-1}^2\left(\frac{\omega_{sat}-\omega_{0,N_j-2}}{z_0}\right) \tag{4.19}$$

➢ For all grid points just behind the right boundary, except end points

$$\frac{d\omega_{N_i-1,j}}{dt} = -\frac{K_r K \rho g \cos\theta}{\mu_0 \varphi}\omega_{N_i-1,j}^2\left(\frac{\omega_{N_i-1,j+1}-\omega_{i,j-1}}{z_{N_i-1}}\right) + \frac{D_0}{\varphi}\left(\frac{\omega_{sat}-\omega_{N_i-2,j}}{(\Delta r)^2}\right)^2 + \frac{D_0\omega_{N_i-1,j}}{\varphi}\left(\left(\frac{1}{r_{N_i-1}}\frac{\omega_{sat}-\omega_{N_i-2,j}}{(\Delta r)^2}\right)+\left(\frac{\omega_{sat}-2\omega_{N_i-1,j}+\omega_{N_i-2,j}}{(\Delta r)^2}\right)\right); \quad 0 < j < N_j - 1 \tag{4.20}$$

➢ For bottom corner grid point on the right boundary

$$\frac{d\omega_{N_i\text{-}1,0}}{dt} = -\frac{K_r K \rho g \cos\theta}{\mu_0 \varphi}\omega^2_{N_i\text{-}1,0}\left(\frac{\omega_{N_i\text{-}1,1}-\omega_{sat}}{z_{N_i\text{-}1}}\right)+\frac{D_0}{\varphi}\left(\frac{\omega_{sat}-\omega_{N_i\text{-}2,0}}{(\Delta r)^2}\right)^2 + \frac{D_0\omega_{N_i\text{-}1,0}}{\varphi}\left(\left(\frac{1}{r_{N_i\text{-}1}}\frac{\omega_{sat}-\omega_{N_i\text{-}2,0}}{(\Delta r)^2}\right)+\left(\frac{\omega_{sat}-2\omega_{N_i\text{-}1,0}+\omega_{N_i\text{-}2,0}}{(\Delta r)^2}\right)\right) \quad (4.21)$$

➢ For top corner grid point on the right boundary

$$\frac{d\omega_{N_i\text{-}1,N_j\text{-}1}}{dt} = -\frac{K_r K \rho g \cos\theta}{\mu_0 \varphi}\omega^2_{N_i\text{-}1,N_j\text{-}1}\left(\frac{\omega_{sat}-\omega_{N_i\text{-}1,N_j\text{-}2}}{z_{N_i\text{-}1}}\right)+\frac{D_0}{\varphi}\left(\frac{\omega_{sat}-\omega_{N_i\text{-}2,N_j\text{-}1}}{(\Delta r)^2}\right)^2 + \frac{D_0\omega_{N_i\text{-}1,N_j\text{-}1}}{\varphi}\left(\left(\frac{1}{r_{N_i\text{-}1}}\frac{\omega_{sat}-\omega_{N_i\text{-}2,N_j\text{-}1}}{(\Delta r)^2}\right)+\left(\frac{\omega_{sat}-2\omega_{N_i\text{-}1,N_j\text{-}1}+\omega_{N_i\text{-}2,N_j\text{-}1}}{(\Delta r)^2}\right)\right) \quad (4.22)$$

➢ For all grid points (excluding corners) on the lower boundary

$$\frac{d\omega_{i,0}}{dt} = -\frac{K_r K \rho g \cos\theta}{\mu_0 \varphi}\omega^2_{i,0}\left(\frac{\omega_{i,1}-\omega_{sat}}{z_i}\right)+\frac{D_0}{\varphi}\left(\frac{\omega_{i+1,0}-\omega_{i\text{-}1,0}}{(\Delta r)^2}\right)^2 + \frac{D_0\omega_{i,0}}{\varphi}\left(\left(\frac{1}{r_i}\frac{\omega_{i+1,0}-\omega_{i\text{-}1,0}}{(\Delta r)^2}\right)+\left(\frac{\omega_{i+1,0}-2\omega_{i,0}+\omega_{i\text{-}1,0}}{(\Delta r)^2}\right)\right) \quad ; 0<i<N_i-1 \quad (4.23)$$

➢ For all grid points (excluding corners) on the upper boundary

$$\frac{d\omega_{i,N_j\text{-}1}}{dt} = -\frac{K_r K \rho g \cos\theta}{\mu_0 \varphi}\omega^2_{i,N_j\text{-}1}\left(\frac{\omega_{sat}-\omega_{i,N_j\text{-}2}}{z_i}\right)+\frac{D_0}{\varphi}\left(\frac{\omega_{i+1,N_j\text{-}1}-\omega_{i\text{-}1,N_j\text{-}1}}{(\Delta r)^2}\right)^2 + \frac{D_0\omega_{i,N_j\text{-}1}}{\varphi}\left(\left(\frac{1}{r_i}\frac{\omega_{i+1,N_j\text{-}1}-\omega_{i\text{-}1,N_j\text{-}1}}{(\Delta r)^2}\right)+\left(\frac{\omega_{i+1,N_j\text{-}1}-2\omega_{i,j}+\omega_{i\text{-}1,N_j\text{-}1}}{(\Delta r)^2}\right)\right) \quad ; 0<i<N_i-1 \quad (4.24)$$

Where $\omega_{i,j}$ is the mass fraction of the gas at the node, (i, j) corresponding to the coordinate, (r, z). $(\Delta r, \Delta z)$ are the distances between equispaced grid points respectively along r and z directions.

The change of the bitumen height at any time is given by the following equations:

$$\frac{dZ_i}{dt} = -v_{i,0} = -\frac{K_r K \rho g \cos\theta}{\mu_0 \varphi}\left(\frac{\omega_{i,0} + \omega_{i+1,0} + 2\omega_{sat}}{4}\right)^2 \quad ; \quad 0 < i < N_i - 1 \tag{4.25}$$

$$\frac{dZ_0}{dt} = -\frac{K_r K \rho g \cos\theta}{\mu_0 \varphi}\left(\frac{\omega_{0,0} + 3\omega_{sat}}{4}\right)^2 \tag{4.26}$$

Δr is constant, and is given by

$$\Delta r = \frac{R}{N_i} \tag{4.27}$$

Δz_i varies with time along r-direction, and is given by

$$\Delta z_i = \frac{Z_i}{N_j} ; \quad 0 \le j \le N_j \tag{4.28}$$

Equations (4.16) - (4.26) were numerically integrated using semi-implicit Bader-Deuflhard algorithm, and adaptive step size control (Press et al., 2001). Analytical Jacobins of equations (4.16) - (4.26) were employed for integration and steepest decent method was used to refine the dispersion coefficient D_0 and minimize the error. To fix the number of grid points, N_i and N_j, the equations were integrated with increasing number of grid points until the change in solution became negligible.

Table (4.1) shows the parameters used in the simulation of the mathematical model.

The cumulative mass of live oil produced at any point is given by the following equation:

$$m_{cal} = 2\pi\rho \sum_{i=0}^{N_i-1} (Z - Z_i) r_{i+1} \Delta r \; ; \quad 0 < i < N_i - 1 \tag{4.29}$$

The algorithm was programmed to generate m_{cal} at the experimental time instants to be compared with its counter part experimental values m_{exp}

The error between the calculated and experimental values was calculated by using root mean square functional as follows:

$$e_{rms} = \sqrt{\frac{1}{N}\sum_{i=1}^{N-2}\left(1-\frac{m_{cal,i}}{m_{exp,i}}\right)^2} \tag{4.30}$$

In equation (4.30), N is the number of the experimental data points, and i denotes the i^{th} experimental time instant.

4.4 Determination of the Dispersion Coefficient

The dispersion coefficient of the solvent gas was considered as a linear function of its concentration in the porous medium as follows:

$$D = D_0\omega \tag{4.31}$$

The previous study (Ronak et al., 2006) has shown this model to yield good agreement between the experimental and model predicted output. Using Equation (4.31) with an initial guess value of D_0, the discretized mathematical model [Equations (4.16)–(4.28)] was solved to yield the calculated mass of oil produced, i.e. m_{cal} [Equation (4.29)], at the experimental time instants. This step leads to the calculation of the root-mean-squared error, e_{rms} given by Equation (4.30). Steepest descent method was used to iteratively improve D_0 and minimize the error. Finite difference approximation was used to calculate the gradient of the error with respect to D_0, which is given by

$$\left[\frac{de_{rms}}{dD_0}\right]_i = \frac{e_{rms,i+1}-e_{rms,i}}{D_{0,i+1}-D_{0,i}} \tag{4.32}$$

where $i \geq 0$ is the iteration counter. For $i=0$, $e_{rms,1}$ was calculated using $D_{0,1} = 0.01D_{0,0}$ where $D_{0,0}$ is the initial guess value of D_0. For any $i \geq 0$, the iterative improvement in the value of D_0 was given by

$$D_{0,i+1} = D_{0,i} - \Delta D_{0,i} \tag{4.33}$$

In the above equation, $\Delta D_{0,i}$ is the change in $D_{0,i}$, which was calculated as follows:

$$\Delta D_{0,i} = \min\left\{10^{-3}\left[\frac{de_{\text{rms}}}{dD_0}\right]_i,\ 0.05D_{0,i}\right\} \tag{4.34}$$

Equation (4.33) avoids a large change in $D_{0,i}$ by restricting it within 5% of its value. If the new $D_{0,i+1}$ increased the error $e_{\text{rms},i+1}$, then the algorithm was backtracked. In that situation, $D_{0,i+1}$ was recalculated using the previous value $D_{0,i}$, but with half of the previous change, i.e. $0.5\Delta D_{0,i}$. The change was halved in succession until the error $e_{\text{rms},i+1}$ decreased or converged to the previous error $e_{\text{rms},i}$. In the latter case, the algorithm converged. In the former case, the iteration of the algorithm proceeded with sequential improvements in D_0 and reductions in the error. The algorithm was programmed to terminate when either the error, or the change in it became less than or equal to 10^{-4}. The optimal D_0 was determined at that point.

The above algorithm is very computationally intensive because a large number of finite-differenced ordinary differential equations and the associated Jacobian evaluations are needed to obtain accurate solutions. Implemented on a 64-bit Itanium computer, the algorithm took about 8 h to converge. The error values at the convergence were of the order 10^{-2}.

Parameters	Value
g, [cm/s²]	981
N_i	25
N_j	10
D_0, [cm²/s] x 10^3	0.194 – 1.39
ω_{sat}	0.70 – 1.0
K [cm²/s]	1.0857×10^{-6} 1.54959×10^{-6} 1.7766×10^{-6}
K_r	1
t [h]	3
R [cm]	3
Z [cm]	21
θ [rad]	90
μ_0 [g/cm.min]	0.797170
ρ [g/cm³]	0.86
$\emptyset$	0.38

Table 4.1 Parameters Used for Model Simulation

5 Results and Discussion

This chapter presents the different values of dispersion coefficient of butane gas which was calculated as a function of gas concentration in Athabasca bitumen for three different permeability packing. As mentioned previously, for each model, an experiment was conducted at a room temperature with ± 0.5 °C variation, and pressure close to butane dew point with variation $\pm$ 0.007 MPa. Under these conditions the cumulative production mass of live oil was measured and recorded every 1 minute (Appendix D). The average of live oil viscosity, density and butane mass fraction in Athabasca bitumen sample were determined as 2.742 cP, 0.86 g/cm^3, and 0.48 respectively.

The values of the live oil viscosity, density and butane mass fraction in Athabasca bitumen sample were in a good agreement with the corresponding values reported earlier by researchers from University of Waterloo Table (2.3).

Root mean square errors were obtained by solving equations (4.15) - (4.30) with various values of D_0 and ω_{sat} in the range of (0.194 – 1.39) x 10^3 cm^2/s and 0.70 – 1.00 respectively. With the iterative refinement in dispersion coefficients D_0, using steepest decent method, the e_{rms} values decrease monotonically to a low values of 0.028, 0.038, and 0.036 with corresponding optimal values of dispersion coefficients 9.4 x 10^{-4}, 9.5 x 10^{-4}, and 9.8 x 10^{-4} cm^2/s for permeability 180, 157, and 110 Darcy respectively (Figure 5.1) and butane saturation mass fraction of 0.71.

The calculated dispersion coefficient values are slightly increased with the decrease of the glass beads size. This is due to the bridging by the particles and the microscopic packing irregularity which occur more frequently as the size of glass beads decreases and the particle shape becomes more irregular as shown in Figure (5.2). The affects of the inhomogenetity of the particles sizes in dispersion coefficients was reported earlier by Perkins and Johnston (1963) and Boustani and Maini (2001) in their analytical models of dispersion equations (2.12), (2.13), (2.16), and (2.17).

There is no much work to date has been reported in butane gas diffusivity and dispersion

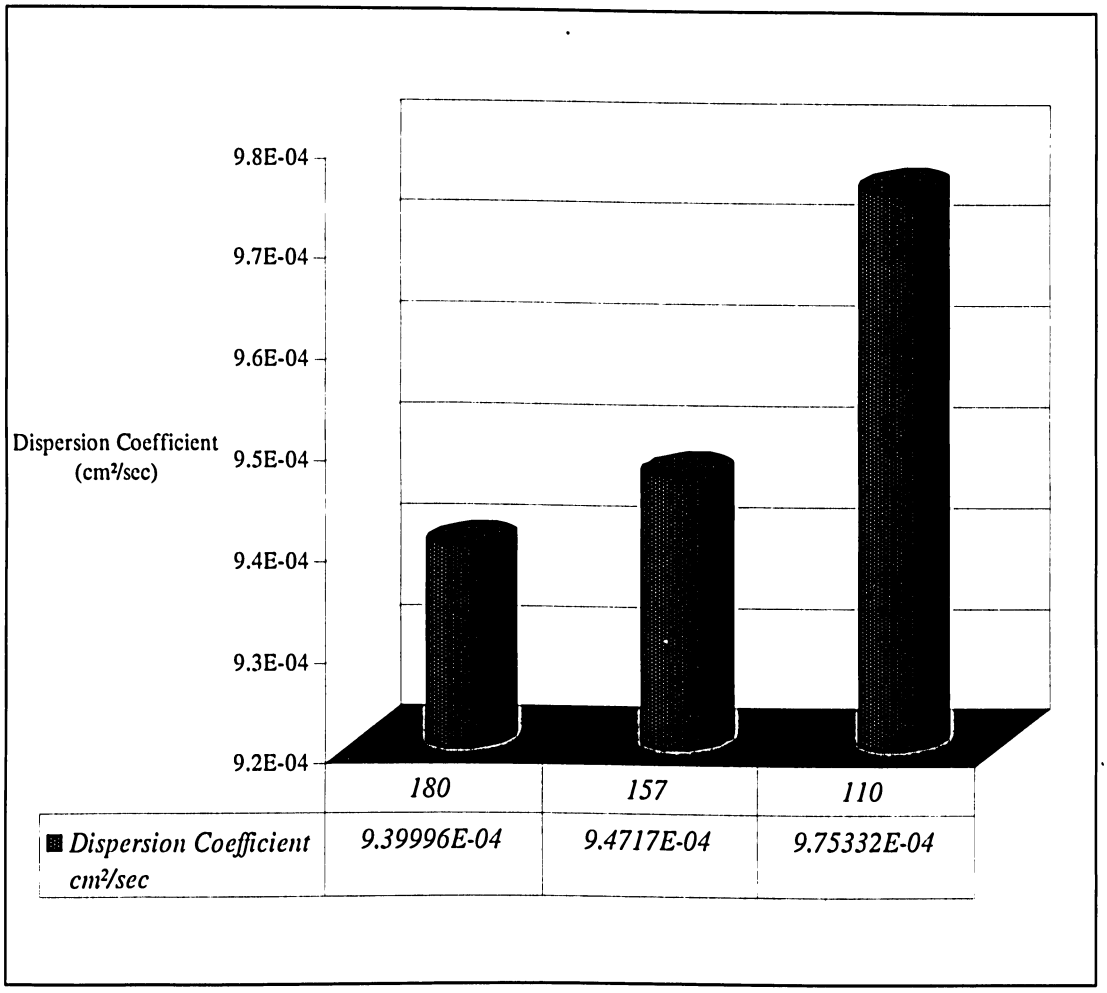

Figure 5.1 Comparison between dispersion coefficients values for different permeability

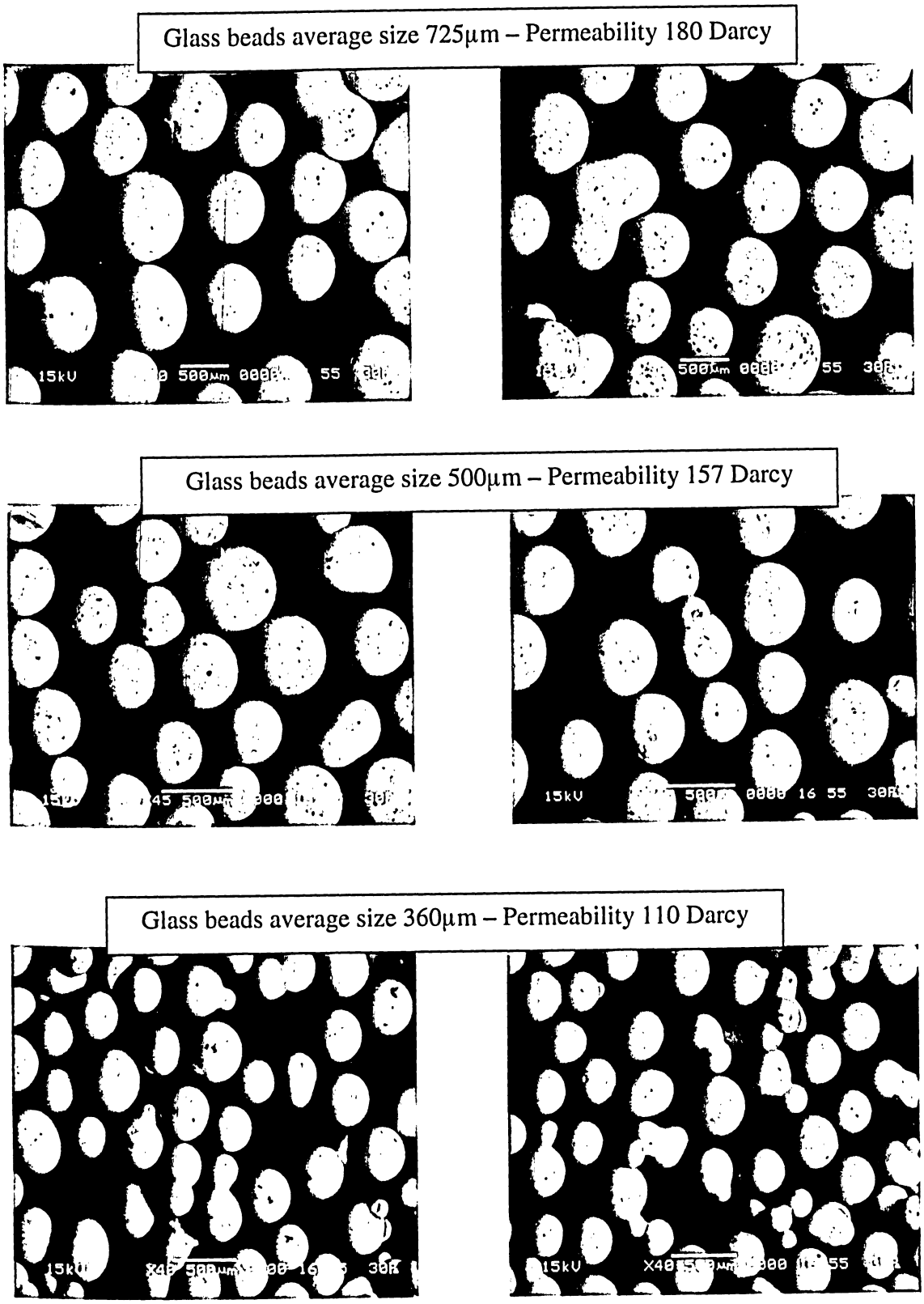

Figure 5.2 Irregularity of Sizes in Small Glass Beads

coefficients in heavy oil and bitumen. The optimal values of dispersion coefficient obtained in this work are two orders of magnitude lower than the dispersion coefficient of butane gas that was numerically determined by Kapadia et al. (2006). The dispersion coefficient is a function of concentration and depending on the live oil viscosity and the solubility limit of solvent under prevailing pressure and temperature. Thus, the difference between optimal dispersion coefficient values obtained on this work and the earlier reported by Kapadia et al. (2006) is due to two factors (i) bitumen viscosity, which is higher in this work by almost one order of magnitude than the one used earlier and (ii) Saturation mass fraction of butane in this work was determined as 0.71, which is lower by 0.16 than the one used by Kapadia (2004). Depending on the solubility limit of the solvent under prevailing pressure and temperature, the diffusion coefficients can change by almost two orders of magnitude (Boustani and Maini, 2001).

Also these optimal values of dispersion coefficient obtained are three orders of magnitude higher than the corresponding molecular diffusion coefficient of butane gas reported by James L. A. et al. (2003) which makes these values of dispersion coefficient fall on the range of effective diffusivity as 2-3 orders of magnitude higher than molecular diffusivity reported earlier by Lim et al. (1996).

These high values of the dispersion coefficient compared to earlier reported diffusion coefficient of butane gas underline the role of convection and surface renewal on Vapex production rates and it justifies the lower predicted production rates than the experimental production rates as claimed by several authors which used molecular diffusion in their mathematical models to predict the production in Vapex.

Predicted live oil production versus time for the optimal values of dispersion coefficient is compared with their experimental counterparts in Figures (5.3) - (5.5). The live oil production started 25-30 minutes following solvent injection. It is observed that the cumulative predicted production is in a good agreement with the cumulative experimental production during the first three hours of production. After the three-hour period, the difference between the calculated and experimental production rates increases. This

behavior is very likely due to the dominance of capillary forces that is not considered in the mathematical model (Appendix E).

The variations of bitumen height in the porous medium with respect to radius at different times for the different optimal values of D_0 are represented in Figures (5.6) - (5.8). As production started, the diluted oil drains under the action of gravity. Once it drains, another surface of heavy oil will be exposed to gas. The surface renewal occurred due to bulk motion.

The physical model was exposed to the gas from top and all the circumference of cylinder. Once the diluted live oil drains under the action of gravity, the butane gas replaces the volume vacated by oil. From Figures (5.6) - (5.8), which illustrate the vertical right side of the cylindrical physical model, the dispersion takes place in a half oblate spheroid shape.

Figures (5.6) - (5.8) also reflecting the change in the bitumen sample height with respect to its radius for three different permeability packing (110, 157 and 180 Darcy). From the graphs the change in height with respect to the radius is directly proportional to the dispersion coefficient.

The dispersion of butane in Athabasca bitumen for the three different permeability packing is expressed by the following relations

For 110 Darcy:

$$D = 9.8 \times 10^{-4} \omega \ (cm^2/s) \qquad (5.1)$$

For 157 Darcy:

$$D = 9.5 \times 10^{-4} \omega \ (cm^2/s) \qquad (5.2)$$

For 180 Darcy:

$$D = 9.4 \times 10^{-4} \omega \ (cm^2/s) \qquad (5.3)$$

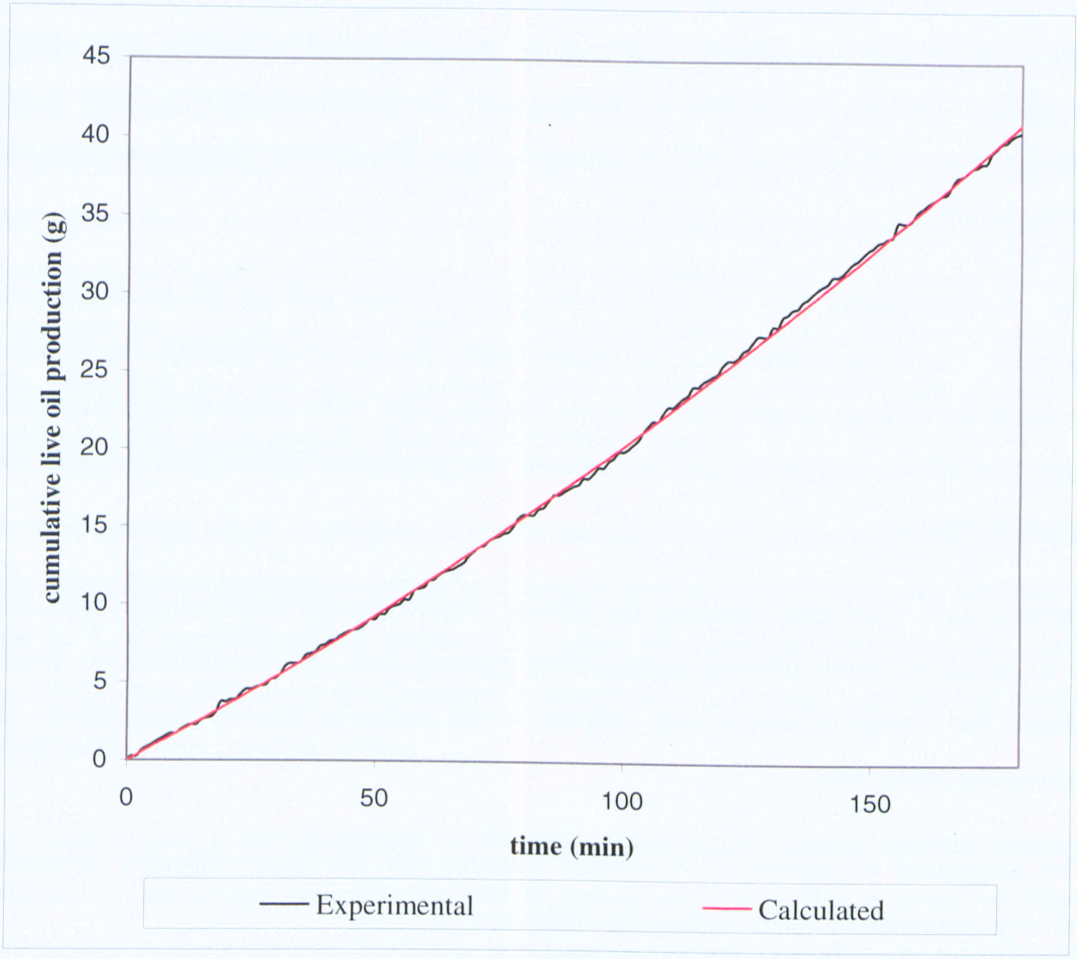

Figure 5.3 Calculated and Experimental Cumulative Mass of Live Oil versus Time (Premeability 110 Darcy)

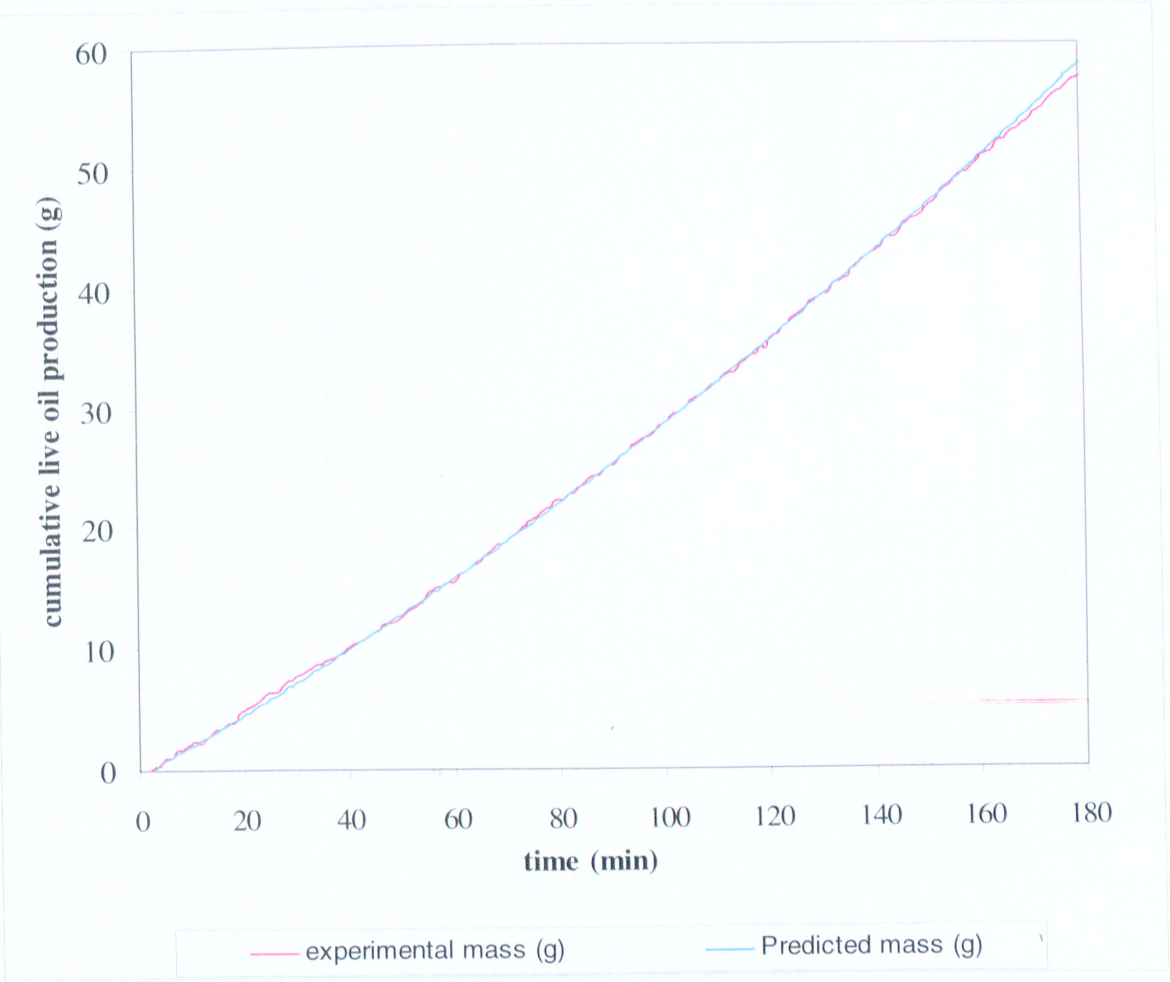

Figure 5.4 Calculated and Experimental Cumulative Mass of Live Oil versus Time (Premeability 157 Darcy)

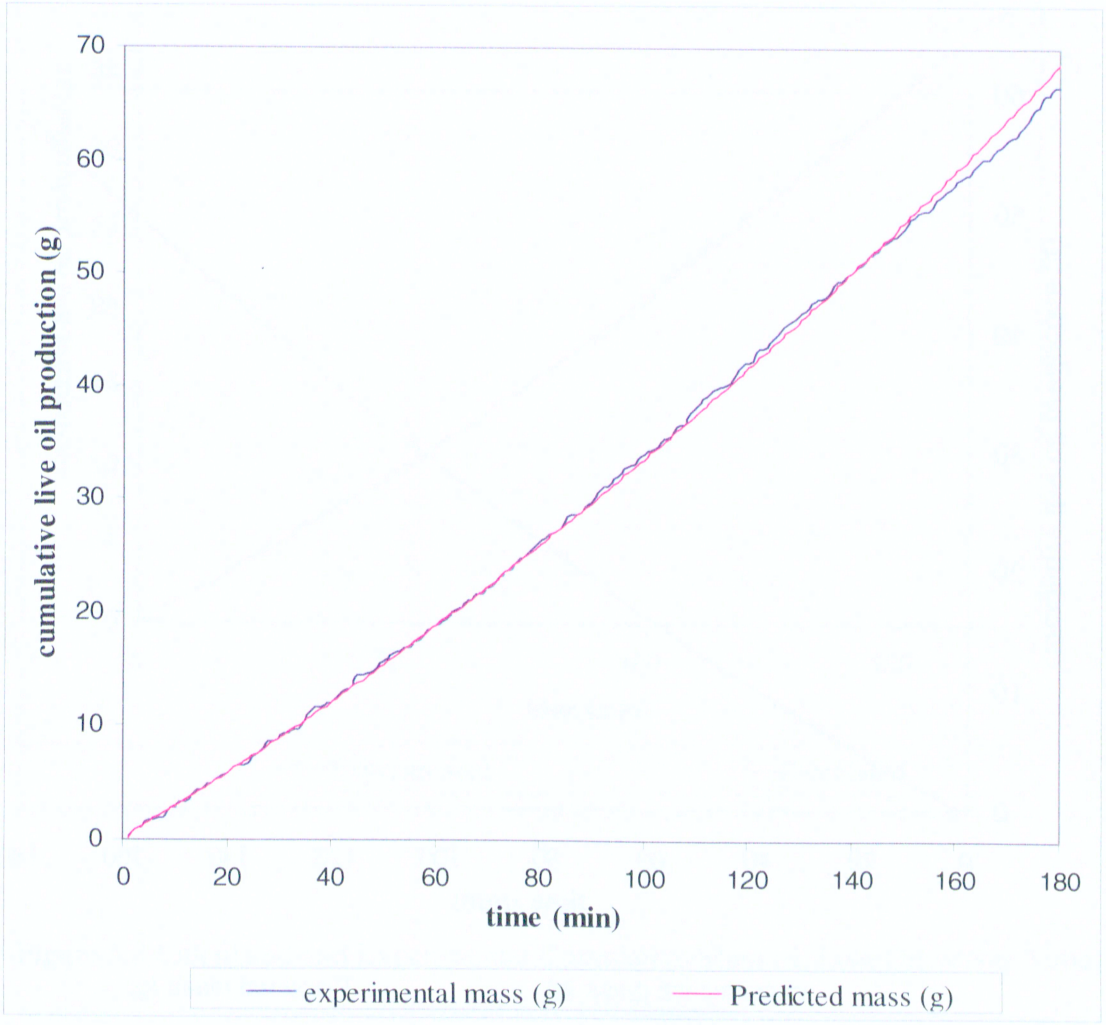

Figure 5.5 Calculated and Experimental Cumulative Mass of Live Oil versus Time (Premeability 180 Darcy)

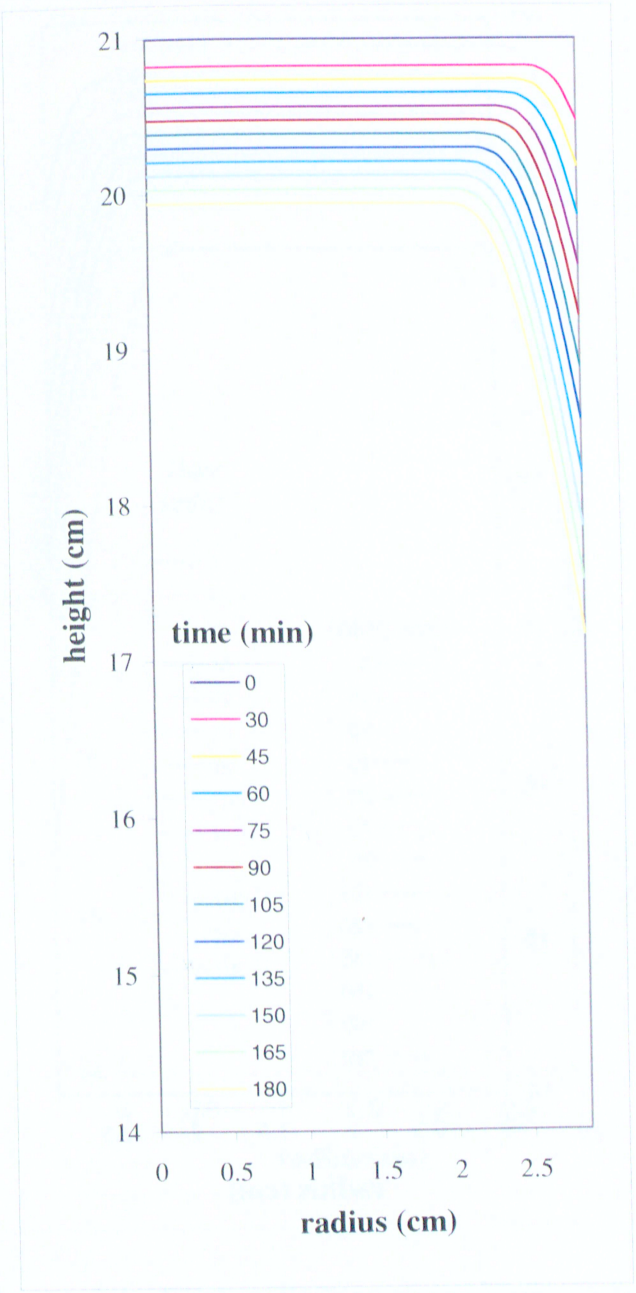

Figure 5.6 Height of the Bitumen Packing versus Radius at Different Times (Permeability 110 Darcy)

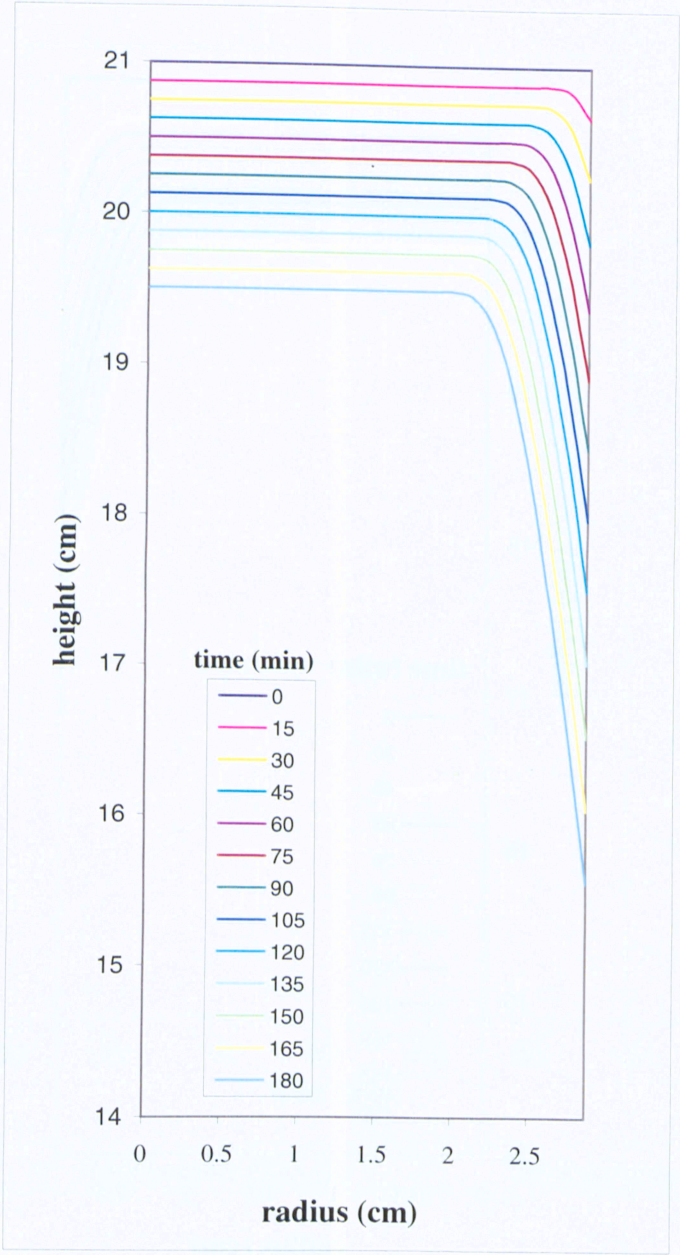

Figure 5.7 Height of the Bitumen Packing versus Radius at Different Times (Permeability 157 Darcy)

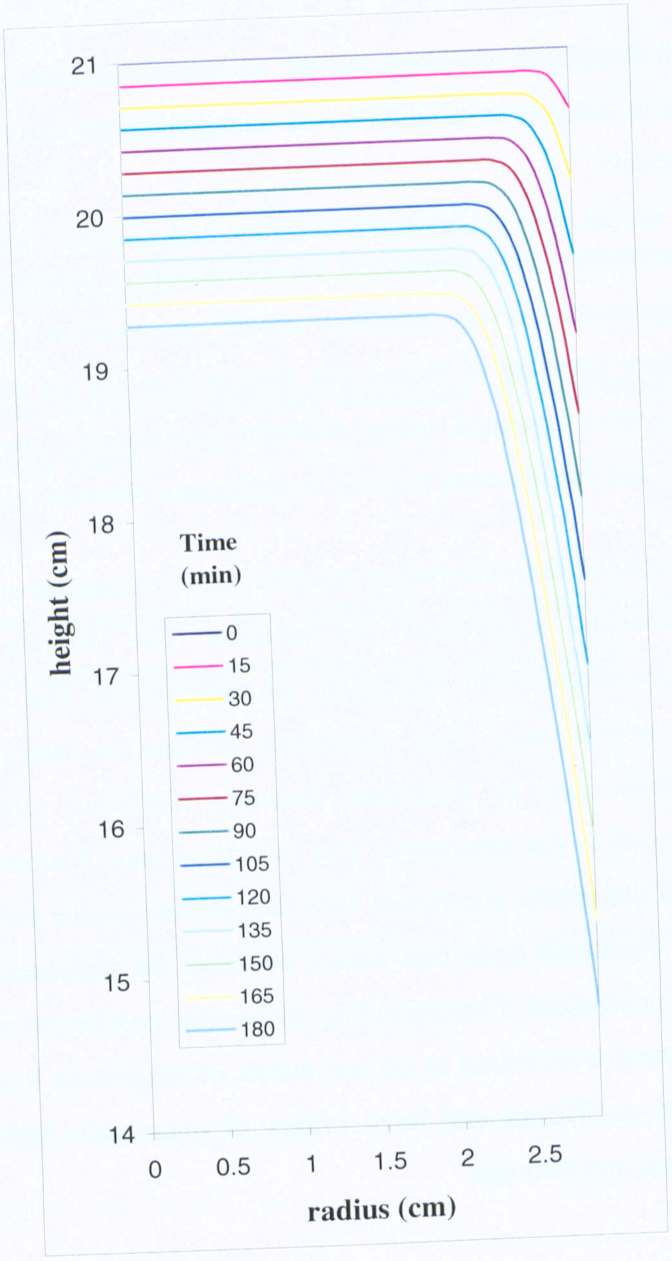

Figure 5.8 Height of the Bitumen Packing versus Radius at Different Times (Permeability 180 Darcy)

6 Conclusion

In this thesis, the dispersion of butane solvent gas was determined as a linear function of its concentration in Athabasca bitumen based on experiments carried out in a laboratory scale physical model.

A series of experiments were performed for extraction of bitumen from a cylindrical saturated homogeneous porous physical model at ambient temperature and the corresponding vapor pressure of butane gas. Sets of data for the cumulative production mass of live oil were obtained using different permeability packing. The Live oil viscosity, density, and butane mass fraction in Athabasca bitumen were also determined.

A mathematical model was developed to describe vapor extraction of Athabasca bitumen experiments at constant temperature and pressure. The bitumen viscosity and gas dispersion were considered to be dependant on composition. The mathematical model was numerically solved using finite difference method to determine the dispersion coefficient of butane gas in Athabasca bitumen. Different values for dispersion coefficients were used in the simulation. The saturation mass fraction of butane and the optimum values of dispersion coefficient were determined on the basis of the minimum root mean square fractional error that occurs between the simulated and experimental values of live oil production. Corresponding dispersion coefficient values of butane in heavy oil and bitumen were found to be two orders of magnitude lower than previously reported dispersion coefficient and three orders of magnitude higher than molecular diffusion in heavy oil and bitumen.

7 Recommendations for Future Work

- Obtain dispersion coefficient of butane gas into heavy oil and bitumen for different physical model length.

- Expanding the mathematical model to incorporates flow of the oil to the surface in both r and z directions.

- Investigate the affects of different conditions on dispersion coefficient using different solvent gases.

Although laboratory experiments are extremely time consuming, measurement of dispersion by experimental techniques provides more reliable result.

Bibliography

Butler, R. M. and Mokrys, I. J., 1989. Solvent Analog Model of Steam Assisted Gravity Drainage. OASTRA Journal of Research, 5 (1): 17-32.

Butler, R. M. and Mokrys, I. J., 1998. Closed-loop Extraction Method for the Recovery of Heavy Oils and Bitumens Underlain by Aquifers: The Vapex Process. J. Can. Pet. Tech., 37 (4): 41–50.

Butler, R. M. and Yee, C. T., 2002. Progress in the Insitu Recovery of Heavy Oils and Bitumens. J. Can. Pet. Tech., 41(1):31-40

Bear, J., 1972. Dynamics of Fluids in Porous Media. America Elsevier Publishing, Inc., USA.

Boustani, A. and Maini, B. B., 2001. The Role of Diffusion and Convective Dispersion in Vapour Extraction Process. J. Can. Pet. Tech., 40 (4): 68–77.

Cuthiell, D., McCarthy, C., Frauenfeld, T., Cameron, S. and Kissel, G., 2003. Investigation of the VAPEX Process Using CT Scanning and Numerical Simulation. J. Can. Pet. Tech., 42 (2): 41–49.

Dusseault, B. M., 2002. Cold Heavy Oil Production with Sand in Canadian Heavy Oil Industry, Alberta Department of Energy

Das, S. K., 1995. In Situ Recovery of Heavy Oil and Bitumen Using Vaporized Hydrocarbon Solvents, Ph.D. thesis, Department of Chemical and Petroleum Engineering, University of Calgary, Calgary.

Das, S. K., Butler R. M. 1998. Mechanism of the Vapour Extraction Process for Heavy Oil and Bitumen. J. Pet. Sci. Eng., 21(1): 43–59.

Das, S. K. 2005. Diffusion and Dispersion in the Simulation of VAPEX Process, SPE 97924, SPE International Thermal Operations and Heavy Oil Symposium, 1–3 November, Calgary, Canada.

Das, S., Bachu, S. and Haug, K., 2002. VAPEX — A Unique Canadian Technology. J. Can. Pet. Tech., 41 (8): 32–34.

Das, S. K., 1997. VAPEX: An Efficient Process for the Recovery of Heavy Oil and Bitumen. SPE 37826, SPE International Thermal Operations Symposium held in Backersfield, California, (February 10–12, 1997), reported in The Future of Heavy Oils and Tar Sands.

Das, S. K. and Butler, R. M., 1994a. Effect of Asphaltene Deposition on the Vapex Process: A Preliminary Investigation Using a Hele-Shaw Cell. J. Can. Pet. Tech., 33 (6): 39–45.

Das, S. K. and Butler, R. M., 1994b. Investigation of "Vapex" Process in a Packed Cell using Butane as a Solvent. Canadian SPE/CIM/CANMET International Conference on Recent Advances in Horizontal Well Applications, March 20–23. Paper No. HWC94-97.

Das, S. K. and Butler, R. M., 1996. Diffusion Coefficients of Propane and Butane in Peace River Bitumen. Can. J. Chem. Eng., 74: 985–992.

Dunn, S. G., Neggiger, E. H., and Rajan, V. S. 1989. A Study of Bitumen Recovery by Gravity Drainage Using Low Temperature Soluble Gas Injection. Can. J. Chem. Eng., 67: 978–991.

ISSACS E.E., 2005. The Energy Innovation Network: Fueling an Integrated Energy Future. Petroleum Society's Canadian International Petroleum Conference, June 7– 9, 2005, Calgary.

El-Haj, R., Lohi, A., and Upreti S.R., 2006, Experimental Determination of Solvent Gas Dispersion in Vapex, 56th Canadian Chemical Engineering Conference, October 15–18, Sherbrooke, 2006.

Ghorayeb, K., and Firoozabadi, A., 2001. Features of Convection and Diffusion in Porous Media for Binary System. Journal of Canadian Petroleum Technology, 40 (2): 21–28.

Hayduk, M. and Minhas, B. S., 1982. Correlations for Prediction of Molecular Diffusivities in Liquids. Can. J. Chem. Eng., 60: 295–299.

Hayduk, W., Castaneda, R., Bromfield, H. and Perras, R. R., 1973. Diffusivities of Propane in Normal Paraffin, Chlorobenzene, and Butanol solvents. AIChE Journal, 19 (4): 859–861.

Hiss, T.G and Cussler, E. L., 1973. Diffusion in High Viscosity Liquids. AIChE Journal, 19: 698–703.

James, L. A., Chatzis, I. and Ioannidis, M. A., 2003. Determination of Diffusion Coefficient of Butane in Heavy Oil and Mass Transfer Rate at the Pore Scale in VAPEX. In Petroleum Society's Canadian International Petroleum Conference. Calgary.

Jin, W., 1999. Heavy Oil Recovery Using the Vapex Process. Master's thesis, University of Waterloo, Waterloo.

Kapadia, R., 2004. Experimental Determination of Solvent Gas Dispersion in Vapor Extraction of Heavy Oils & Bitumen, M.A.Sc. thesis, Department of Chemical Engineering, Ryerson University, Toronto.

Kapadia, R., Upreti, S. R., Lohi, A., and Chatzis I., 2006. Determination of Gas Dispersion in Vapor Extraction of Heavy Oil and Bitumen. J. Pet. Sci. Eng. 51(3–4), 214–222.

Latil, M., 1980. Enhanced Oil Recovery. Paris: Editions Technip Lederer, E. L., 1933. Proceedings of World Pet. Cong.

Nghiem, L. X., Kohse, B. F. and Sammon, P. H., 2001. Compositional Simulation of the VAPEX Process. J. Can. Pet. Tech., 40 (8): 54–61.

Oil & Gas Journal, Dec. 19, 2005, U.S. Energy Information Administration. Vol. 103, No. 47 http://www.eia.doe.gov/emeu/international/petroleu.html .

Oballa, V. and Butler, R. M., 1989. An Experimental Study of Diffusion in the Bitumen–Toluene System. J. Can. Pet. Tech., 28: 63–69.

Oduntan, A. R., 2001. Heavy Oil Recovery Using the VAPEX Process: Scale–Up and Mass Transfer Issues. Master's thesis, University of Waterloo.

Oduntan, A. R., Chatzis, I., Smith, J. and Lohi, A., 2001a. Heavy Oil Recovery Using the VAPEX Process: Scale-Up Issues. In 52nd Technical meeting of the Canadian International Petroleum Conference. Calgary.

Oduntan, A. R., Chatzis, I., Smith, J. and Lohi, A., 2001b. Heavy Oil Recovery using the VAPEX Process: Scale-up Issues. Petroleum Society's Canadian International Petroleum Conference, June 12–14, Calgary. Paper 2001-127.

Ramakrishnan, V., 2003. In Situ Recovery of heavy oil by VAPEX using Propane. Master's thesis, University of Waterloo.

Renner, T. A., 1988. Measurement and Correlation of Diffusion Coefficients for CO2 and Rich-gas Applications. SPE Reservoir Eng.: 517–523.

Riazi, M. R., 1996. A New Method for Experimental Measurement of Diffusion Coefficients in Reservoir Fluids. J. Pet. Sci. Eng., 14: 235–250.

Rosman, A. and Zana, E., 1977. Experimental Studies of Low IFT Displacement by CO2 Injection. SPE 6723, SPE 52nd Annual Fall Meeting,October 9–12, Denver.

Perkins, T. K., and Johnston, O. C. 1963. A review of Diffusion and Dispersion in Porous Media, SPE Journal, 3: 70–84.

Schmidt, T., 1989. Mass Transfer by Diffusion. In L. G. Helper, C. Hsi, eds., AOSTRA Technical Handbook on Oil Sands, Bitumens and Heavy Oils. Edmonton, Canada: Alberta Oil Sands Technology and Research Authority, pp. 329-331.

Upreti, S. R., 2000. Experimental Measurement of Gas Diffusivity in Bitumen: Results for CO2, CH4, C2H6, and N2. Ph.D. thesis, Department of Chemical and Petroleum Engineering, University of Calgary, Calgary.

Upreti, S. R. and Mehrotra, A. K., 2000. Experimental Measurement of Gas Diffusivity in Bitumen: Results for Carbon Dioxide. Industrial and Engineering Chemistry Research, 39 (4): 1080–1087.

Upreti, S. R. and Mehrotra, A. K., 2002. Diffusivity of CO_2, CH_4, C_2H_6 and N_2 in Athabasca Bitumen. Can. J. Chem. Eng., 80: 116–125.

Yazdani, J. A., Maini, B. B. 2005. Effect of Drainage Height and Grain Size on Production Rates in the VAPEX Process: Experimental Study, SPE Reservoir Evaluation & Engineering, 8: 205–213.

Appendix A

A. Sample of calculations of different glass beads permeability

The glass beads permeability was calculated by rearranging equation (3.1) and substituting for all the parameters from the (Table A 1).

NB. The differential pressure transducer used to measure Δp has accuracy +/- 0.001 psi.

$$k = \frac{Q\mu}{A}\frac{\Delta L}{\Delta p} \qquad (A-1)$$

$$k = \frac{\left(33.33\,cm^3/s\right)\left(1.84\times10^{-9}\ N.s/cm^2\right)}{28.26\,cm^2}\left(\frac{21\,cm}{4.2\times10^{-2}\ N/cm^2}\right)$$

Glass Beads Average size (μm)	360	500	725
Air flow rate "Q" (cm^3/s)	33.33	33.33	33.33
Cross section area of the glass beads packing "A" (cm^2)	28.26	28.26	28.26
Viscosity of the air "μ" ($N.s/cm^2$) (T=20°C)	1.84×10^{-9}	1.84×10^{-9}	1.84×10^{-9}
Pressure drop "Δp" (N/cm^2)	4.2×10^{-2}	2.94×10^{-2}	2.56×10^{-2}
Length of glass beads packing "ΔL" (cm)	21	21	21
Permeability "k" (cm^2)	1.085×10^{-6}	1.550×10^{-6}	1.777×10^{-6}
Permeability "k" (Darcy)	1.100×10^{2}	1.570×10^{2}	1.800×10^{2}

Table A 1 Data for Glass Beads Permeability Calculations

Appendix B

B. Sample of Live Oil Viscosity Calculations

The live oil viscosity was calculated by rearranging equation (3.2) and substituting for all the parameters from the (Table A 2) (temperature range of 22° – 24° C)

$$\mu(\text{cP}) = \frac{\pi \times d^4 \times \Delta p \times 68948 \times 100}{128 \times Q \times L} \qquad \text{(B.1)}$$

$$\mu(\text{cP}) = \left[\frac{3.14 \times (0.1016)^4 \text{cm}^4 \times 2.8\text{psi}}{128 \times 0.37\,\text{cm}^3/\text{s} \times 50\text{cm}}\right]\left[\frac{68948\text{dyne/cm}^2}{\text{psi}}\right]\left[\frac{100\ \text{cP}}{\text{dyne/cm}^2.\text{s}}\right]$$

Time (min)	volumetric flow rate (cm^3/s)	Pressure Drop Across Capillary Tube (ΔP)	Live Oil Viscosity ($dyne.s/cm^2$)	Live Oil Viscosity (cP)
137	0.37	2.8	0.027	2.742
165	0.29	2.2	0.027	2.738
200	0.28	2.1	0.027	2.742
235	0.38	2.92	0.027	2.734
300	0.4	2.99	0.027	2.724
324	0.32	2.4	0.027	2.733
335	0.39	2.96	0.028	2.756

Table A 2 Data for the Live Oil Viscosity Calculations

Appendix C

C. Sample of Butane Solubility and Live Oil density Calculations

To calculate the butane solubility and live oil density, substitute in equations (3.3) and (3.4) for all the parameters from the (Table A 3)

$$C_4H_{10} \text{ Dissolved weight fraction} = \frac{6.68\ g}{7.46\ g + 6.68\ g} \qquad (C.1)$$

$$\text{Live Oil Density} = \frac{6.68\ g + 7.46\ g}{16.74\ cm^3} \qquad (C.2)$$

Dead Oil Mass (g)	Librated Butane Mass (g)	Live Oil Volume (cm3)	Live Oil Density (g/cm3)	Dissolved Butane Fraction
7.46	6.68	16.74	0.8447	0.47
6.8	6.02	14.96	0.8570	0.47
8.32	6.81	17.45	0.8670	0.45
5.5	5.37	12.82	0.8479	0.49
7.13	7.2	16.38	0.8748	0.5
6.98	6.55	15.67	0.8634	0.48
7.2	6.28	15.67	0.8602	0.47

Table A 3 Data for the Butane Solubility and Live Oil Density Calculations

Appendix D

D. Sample Data for Cumulative Live Oil Production

The cumulative production mass of live oil was measured and recorded every 1 minute. This sample of data represents an averaged for every 3 minutes

Time (min)	Bitumen Sample Weight (g)	Mass of Live Oil (g)	Cumulative Mass of Live Oil weight (g)
0	1282.60	0.000	0.000
3	1281.68	0.924	0.924
6	1280.85	0.828	1.753
9	1280.34	0.510	2.262
12	1279.32	1.020	3.282
15	1278.74	0.574	3.856
18	1277.47	1.275	5.130
21	1276.35	1.115	6.245
24	1275.72	0.637	6.883
27	1274.92	0.797	7.679
30	1274.25	0.669	8.348
33	1273.65	0.605	8.954
36	1272.98	0.669	9.623
39	1272.02	0.956	10.579
42	1271.22	0.797	11.376
45	1270.56	0.669	12.045
48	1269.66	0.892	12.937
51	1268.96	0.701	13.638
54	1267.59	1.370	15.008
57	1266.86	0.733	15.741
60	1265.71	1.147	16.888
63	1264.72	0.988	17.876
66	1263.86	0.860	18.736
69	1262.65	1.211	19.947
72	1261.92	0.733	20.680
75	1260.84	1.083	21.763
78	1260.01	0.828	22.592
81	1259.02	0.988	23.580
84	1258.35	0.669	24.249
87	1257.33	1.020	25.268
90	1256.25	1.083	26.352

Time (min)	Bitumen Sample Weight (g)	Mass of Live Oil (g)	Cumulative Mass of Live Oil weight (g)
93	1255.16	1.083	27.435
96	1254.27	0.892	28.327
99	1253.19	1.083	29.411
102	1252.07	1.115	30.526
105	1251.05	1.020	31.546
108	1250.26	0.797	32.342
111	1249.11	1.147	33.489
114	1248.31	0.797	34.286
117	1246.72	1.593	35.879
120	1245.35	1.370	37.249
123	1244.39	0.956	38.205
126	1243.34	1.052	39.257
129	1242.29	1.052	40.308
132	1240.92	1.370	41.678
135	1240.03	0.892	42.571
138	1238.82	1.211	43.781
141	1237.96	0.860	44.642
144	1237.03	0.924	45.566
147	1235.73	1.306	46.872
150	1234.48	1.243	48.115
153	1233.34	1.147	49.262
156	1232.22	1.115	50.377
159	1231.08	1.147	51.524
162	1229.99	1.083	52.608
165	1229.04	0.956	53.564
168	1227.92	1.115	54.679
171	1226.65	1.275	55.954
174	1225.53	1.115	57.069
177	1224.54	0.988	58.057
180	1223.36	1.179	59.236
183	1222.19	1.179	60.415
186	1221.36	0.828	61.243
189	1220.11	1.243	62.486
192	1218.97	1.147	63.633
195	1217.60	1.370	65.003
198	1216.55	1.052	66.055
201	1215.17	1.370	67.425

Time (min)	Bitumen Sample Weight (g)	Mass of Live Oil (g)	Cumulative Mass of Live Oil weight (g)
204	1213.84	1.338	68.763
207	1212.75	1.083	69.846
210	1211.38	1.370	71.217
213	1210.27	1.115	72.332
216	1209.06	1.211	73.543
219	1207.94	1.115	74.658
222	1206.67	1.275	75.933
225	1205.55	1.115	77.048
228	1204.32	1.235	78.283
231	1203.00	1.315	79.598
234	1202.05	0.948	80.545
237	1201.01	1.040	81.585
240	1199.94	1.070	82.655
243	1198.94	1.001	83.656
246	1197.99	0.954	84.609
249	1196.87	1.118	85.727
252	1195.76	1.115	86.842
255	1194.72	1.037	87.879
258	1193.76	0.965	88.844
261	1192.92	0.832	89.676
264	1192.01	0.909	90.585
267	1191.12	0.895	91.480
270	1190.22	0.900	92.380
273	1189.27	0.954	93.334
276	1188.28	0.984	94.318
279	1187.36	0.926	95.244
282	1186.37	0.984	96.228
285	1185.55	0.826	97.054
288	1184.80	0.748	97.801
291	1183.97	0.831	98.633
294	1183.14	0.826	99.458
297	1182.34	0.800	100.258
300	1181.35	0.996	101.254

Table A 4 Production Data for 157 Darcy Model

Appendix E

E. Results for 5 hours of operation

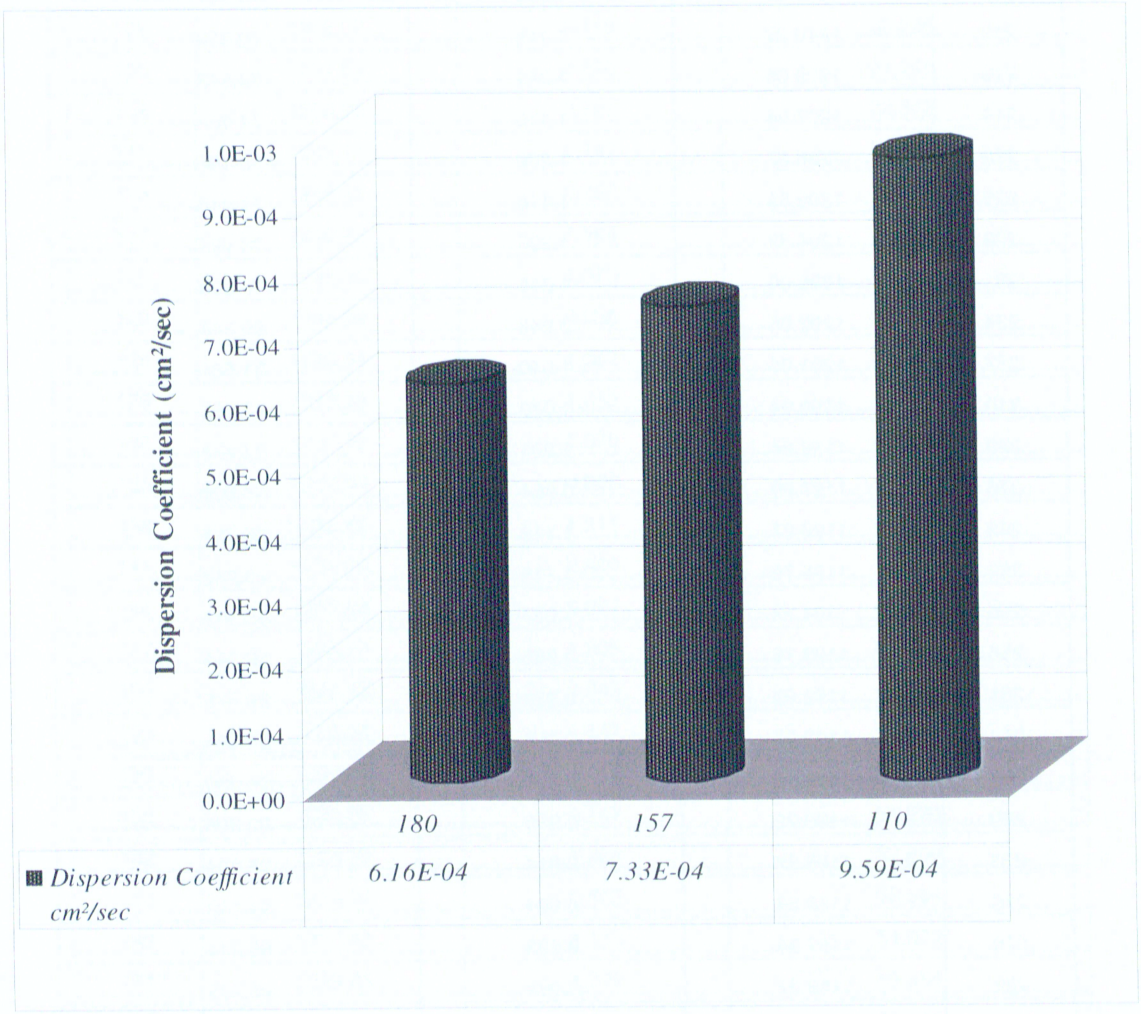

Figure E 1 Comparison between dispersion coefficients values for different permeability (Production time 5 hours)

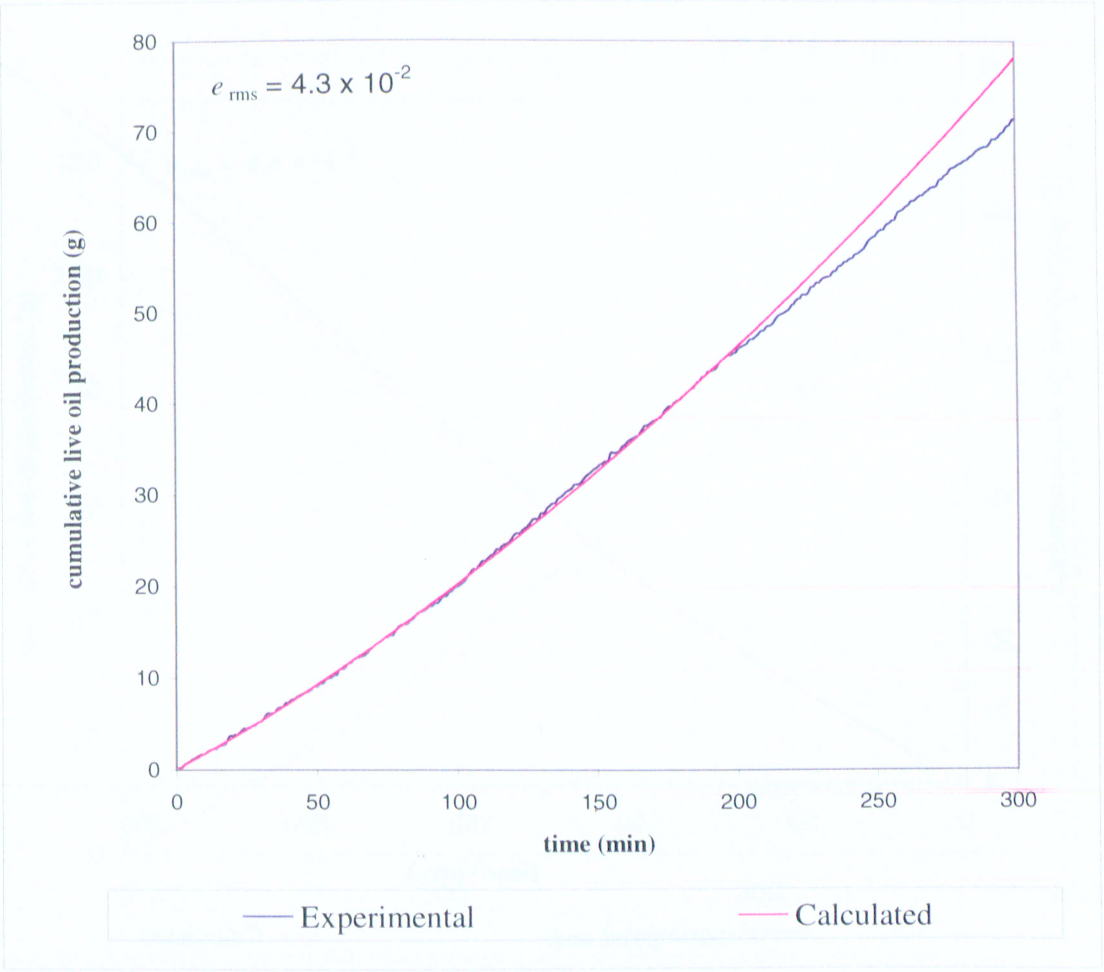

Figure E 2 Calculated and Experimental Cumulative Mass of Live Oil versus Time (110 Darcy – t = 5 h)

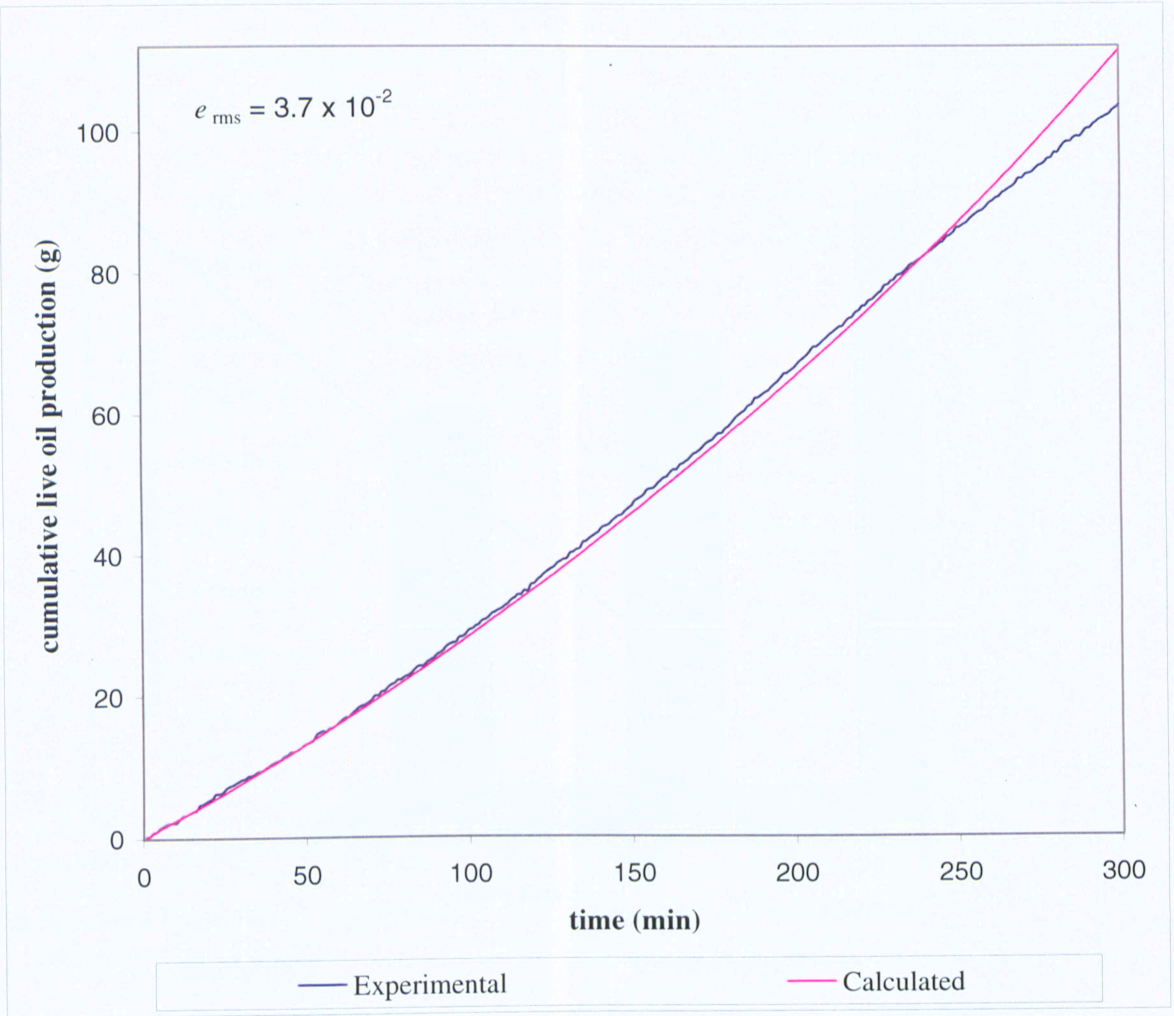

Figure E 3 Calculated and Experimental Cumulative Mass of Live Oil versus Time (157 Darcy – t = 5 h)

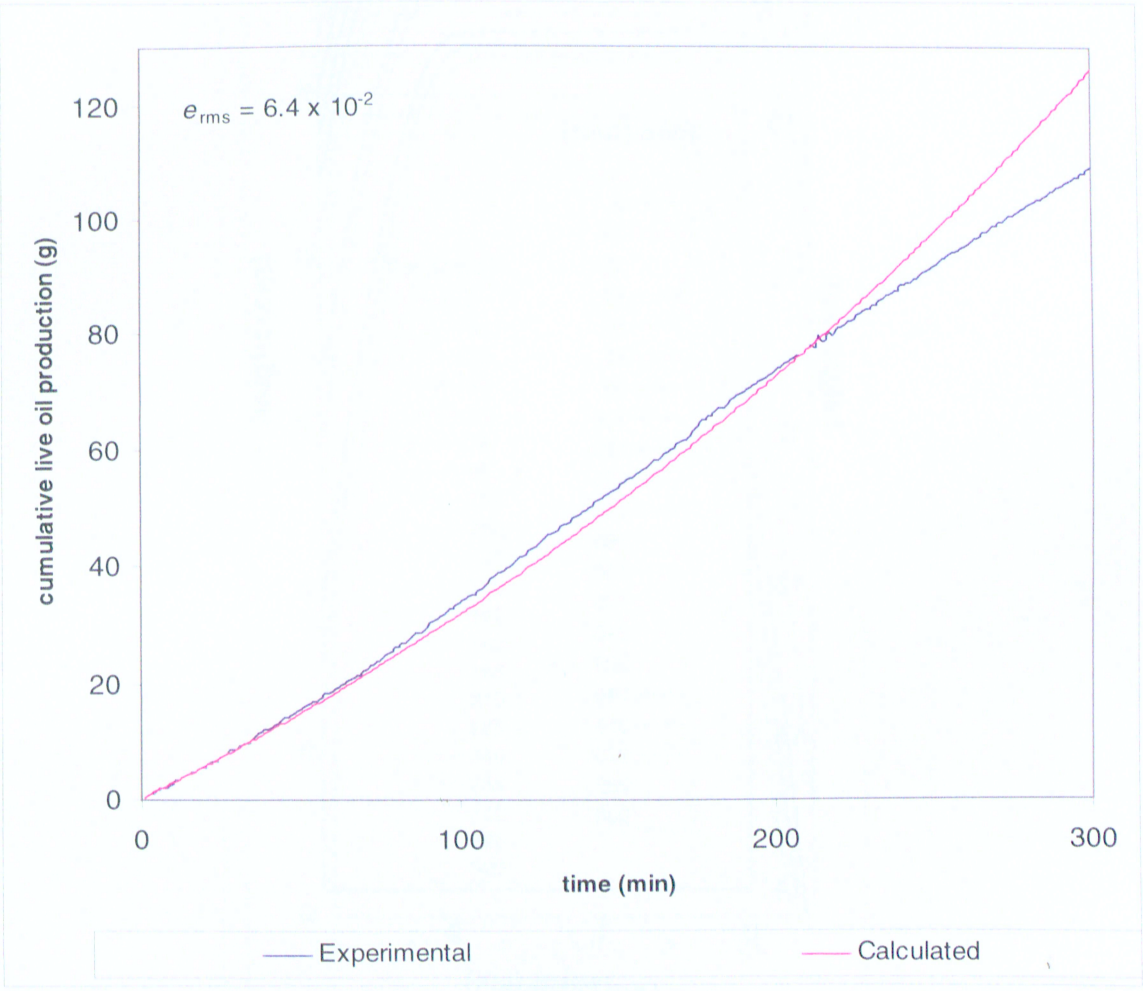

Figure E 4 Calculated and Experimental Cumulative Mass of Live Oil versus Time (180 Darcy – t = 5 h)

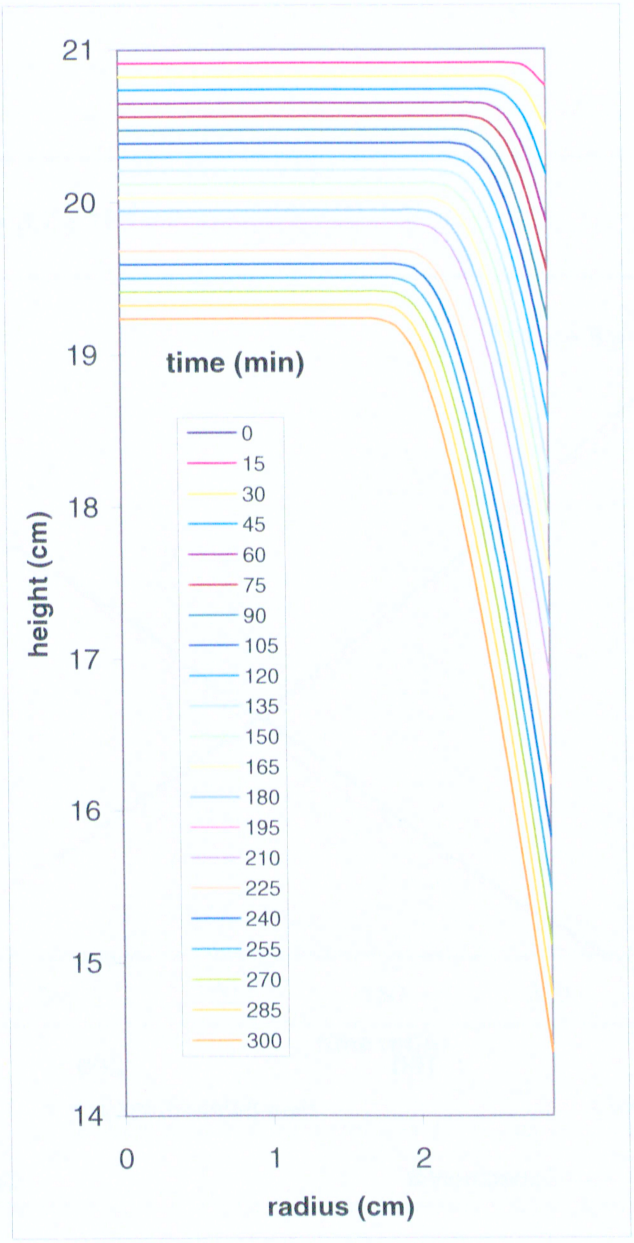

Figure E 5 Height of the Bitumen Packing versus Radius at Different Times

(110 Darcy – t = 5 h)

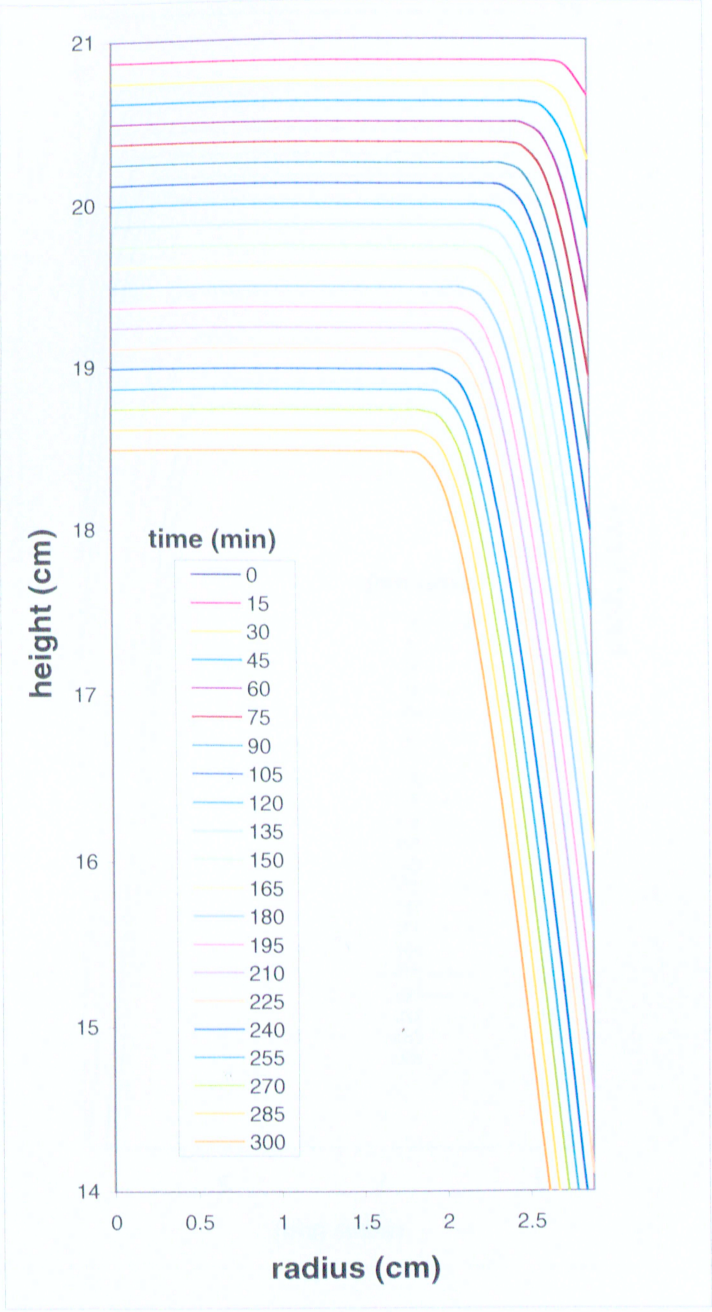

Figure E 6 Height of the Bitumen Packing versus Radius at Different Times (157 Darcy – t = 5 h)

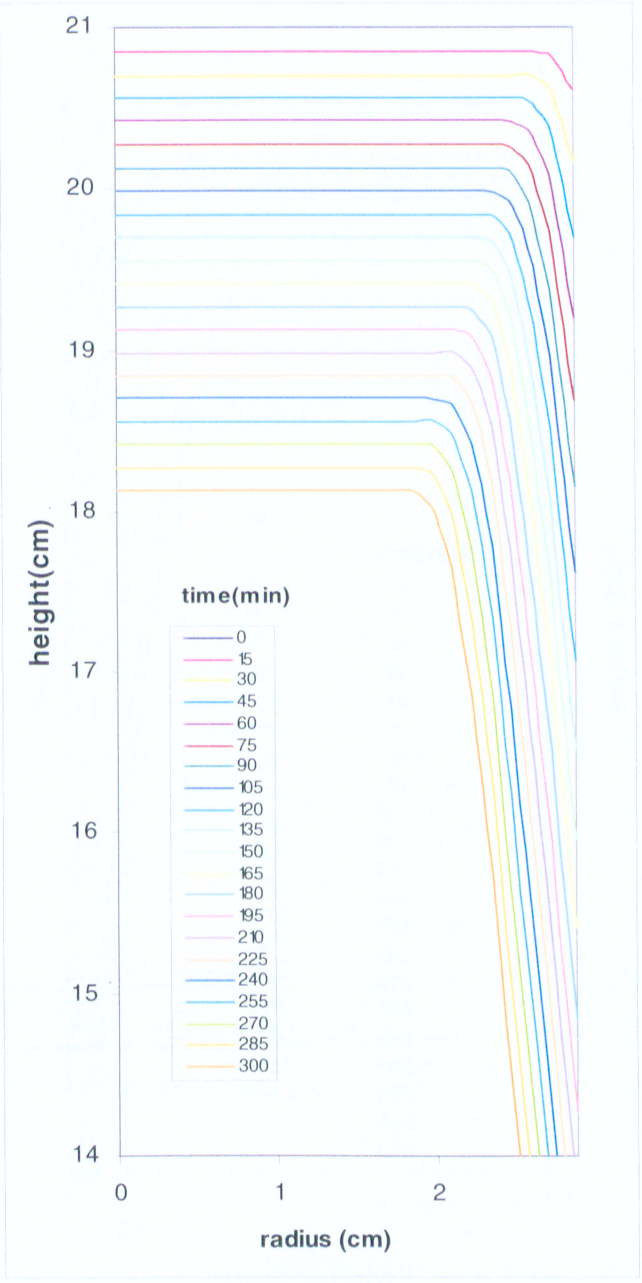

Figure E 7 Height of the Bitumen Packing versus Radius at Different Times

(180 Darcy – t = 5 h)